See-through science: *Danionella cerebrum* as a model for neuroregeneration

Mallika K. Misyuk[1,2], Joseph L. Austin[1,2], Noelle R. Walechka[1,2], Juliet A. Peterka[1,2], Matthew B. Veldman[2,3], Pui-Ying Lam[1,2]

[1]Neuroscience Research Center, Medical College of Wisconsin, 53226 Milwaukee, WI, USA
[2]Department of Cell Biology, Neurobiology and Anatomy, Medical College of Wisconsin, 53226 Milwaukee, WI, USA
[3]Department of Ophthalmology and Visual Sciences, Medical College of Wisconsin, 53226 Milwaukee, WI, USA

Abstract

Rebuilding functional neuronal circuits after injury in the adult central nervous system (CNS) is unachievable for many vertebrates. In pro-regenerative models, it is unclear how regeneration and re-wiring is achieved in the CNS over long distances. The size and opacity of the adult vertebrate brain makes it difficult to study axon topography and dynamic cellular interactions during long-distance axon regeneration. Here, we harnessed the properties of the small and transparent adult *Danionella cerebrum* for longitudinal *in vivo* imaging of retinal ganglion cell axon regeneration, correlating cellular events with functional recovery. Our results suggest that some axons regenerate along tracts of degenerating myelin debris. However, the topography of re-innervation is different after regeneration, suggesting that new axon tracts are created to restore functional vision. The *D. cerebrum* model provides a unique opportunity to visualize and experimentally manipulate the spatial and temporal events during CNS regeneration in intact adult vertebrates.

Introduction

It is well known that after a central nervous system (CNS) injury, most mammals fail to sufficiently regenerate damaged axons to achieve proper target innervation. Long distance axon regeneration after an optic nerve injury has been successfully induced in mice using genetic manipulations[1-4], however, functional recovery of vision fails since axons do not make proper connections. Vision is restored after injury in pro-regenerative models, but it remains unclear how the neuronal topographic map is re-established during regeneration, as well as how axonal remodeling events during late regeneration contribute to functional recovery.

In nerve regeneration studies using vertebrate animals, identifying key morphological events traditionally requires histological sectioning of fixed tissue, and/or tissue clearing[5, 6]. Although optical tissue clearing techniques have enabled three-dimensional imaging of entire organs, imaging dynamic cell-cell interactions, monitoring the same animal over time, and correlating cellular events with functional recovery has not been possible. Alternatively, the use of intra-vital microscopy in the CNS of traditional adult animal models requires the invasive implantation of an imaging window, yet allows for a limited imaging field and depth[7]. To overcome this, larval zebrafish have been used for the *in vivo* study of cellular dynamics and regeneration, owing to their small size and transparency. However, larvae lack complex memory-based behaviors and fully developed endocrine and neuro-immune systems, making it challenging to distinguish between different phases of regeneration and functional recovery or to identify sex-based differences and neuro-immune responses during regeneration[8]. *Danionella cerebrum* (DC) is a new vertebrate model that provides a unique opportunity to visualize the entire brain, *in vivo,* at single cell resolution. Adult DC remain largely optically transparent, have the smallest known brain, and lack a dorsal skull cap[9-21], thereby making DC particularly suitable for imaging cellular dynamics, especially in the CNS, in a live animal without the need for surgical manipulations.

Here, we induced axonal injury in adult DC retinal ganglion cells (RGCs) by adapting an optic nerve crush (ONC) technique that has been used in other animal models to study CNS regeneration[22, 23], and correlated functional recovery with cellular events *in vivo*. We showed that vison in adult DC is functionally restored after RGC axons are regenerated. Imaging revealed that axons regenerated over a long distance and exhibited evidence of axon remodeling. Real-time *in vivo* characterization of regeneration and recovery was facilitated by generating novel DC transgenic reporter lines for axonogenesis and myelinated oligodendrocyte membranes. For longitudinal assessment of RGCs pre- and post-regeneration, we employed a sparse labeling technique using an RGC specific promoter. CRISPR/Cas9 genome editing was used to generate a pigment mutant line to enhance *in vivo* brain imaging. Additionally, two behavior-based assays were developed to assess vision recovery. Using these tools, we found that through axon remodeling events, the regenerated axonal network displayed a topography that was distinct from its pre-injury state. We also observed that a subset of regenerating RGC axons followed degenerating myelin tracts with regenerating axons re-innervating the correct targets, leading to functional vision recovery. The DC model provides new avenues for future studies aimed at understanding how successful CNS regeneration is orchestrated.

Results

Adult D. cerebrum can functionally recover from an optic nerve injury. In non-mammalian vertebrates, retinal ganglion cell axons exit the eye as the optic nerve and innervate the optic tectum (TeO), the largest brain center for visual processing. After an optic nerve injury in zebrafish, approximately 75% of RGCs survive[24] with axonal regeneration[25, 26] leading to functional recovery[27-29]. It is not known if the CNS of adult DC can regenerate. We established the ONC technique in adult DC to inflict a CNS injury (**Fig. 1A-A'**), then assessed their ability

to regain vision using two behavioral assays, a dorsal light response (DLR) and a looming response (LR) assay. The DLR assay has been used to assess vision in fish. When vision is lost in one eye, fish tend to tilt their body such that the eye that has lost vision tilts upwards. The recovery of head tilt correlates with the recovery of vision[27-31]. Based on this principle, we devised a DLR assay for adult DC to accommodate their small size and transparency for video recording and analysis (**Fig. 1B, Extended Data 1A, Methods**). After subjecting *wild-type* (*WT*) animals to an ONC, we measured the head tilt angle over the course of 18 days (**Fig. 1B' and 1C**). Compared to pre ONC, a significant change in head tilt angle was observed at 1-day post ONC (dpONC; **Fig. 1D**). Head tilt angle recovered by 18 dpONC, suggesting that adult DC can recover vision after an ONC (**Fig. 1D, Suppl. Video 1**). When comparing the recovery of males to females, there was no significant difference except at 10 dpONC.

To evaluate the functional vision of injured DC, we established an LR assay (**Fig. 1E-F, Extended Data 1B**). This assay tests the ability of fish to detect a predatory stimulus and has been used to assess visual function[32, 33]. Fish can display an escape behavior in response to a looming stimulus with only one eye. To specifically assess vision recovery from the ONC-injured eye, the optic nerve of one eye was first transected, then an ONC was performed on the other eye one day later (**Fig. 1G**). We used the DLR assay to validate that vision did not recover after a full optic nerve transection (ONT) in adult DC (**Extended Data 2**). The percentage of fish responding to a looming stimulus at 1 dpONC was significantly lower compared to those responding pre-injury (**Fig. 1H**). Vision recovery was observed at 8 dpONC, although the percentage of fish responding was still lower than at pre ONC levels (**Fig. 1H, Suppl. Video 2**). The time to recover from ONC, as determined using the DLR assay differed from the LR assay. This might be due to the different synaptic connections required to elicit different visual responses as it was shown that teleost fish use different visual pathways when responding to different visual cues.[34] Nonetheless, our results show adult DC can recover from an ONC injury, the progress of which can be assessed using DLR and/or LR assay.

An axonogenesis reporter line for adult fish. To facilitate the *in vivo* visualization of regenerating axons, we generated a novel transgenic DC line, *Tg(gap43:mGreenLantern-CAAX)*. Previous work has shown that the *gap43* promoter from Japanese pufferfish, *Takifugu,* can be used to track neuronal development and regeneration in zebrafish[26]. At early developmental stages (2-days post fertilization; dpf), robust *gap43* promoter-driven expression in the brain and eye was observed (**Fig. 2A-D, 2A'-D', Extended Data 3**) and persisted into the young adult stage (2.5 months post fertilization; mpf) (**Fig. 2E-E'**). *gap43* promoter-driven expression was detected in different regions of the forebrain, midbrain, and hindbrain at all depths imaged, from the dorsal plane through to the ventral plane (**Fig. 2G-I, 2G'-I', Suppl. Video 3**). These observations demonstrated that this *gap43* promoter-based transgenic line shows expression throughout the brain and allows for monitoring of neurogenesis in the entire brain of adult DC.

The expression of the endogenous *gap43* gene is downregulated as the animal ages due to the conclusion of neurogenesis[35, 36]. We performed longitudinal imaging experiments on the same *Tg(gap43:mGreenLantern-CAAX)* animals to quantify levels of *gap43* promoter-driven expression in multiple brain regions (**Extended Data 4A**). We observed significant downregulation of *gap43* reporter signal in all 3 regions of the brain at 6.5 mpf as compared to 2 mpf. Although levels had decreased in all regions tested, we could still detect signal at 6.5 mpf (**Extended Data 4B-J**), suggesting that fish at this age continue to exhibit some degree of neurogenesis.

Axon regeneration in vivo. To visualize RGC axon regeneration *in vivo*, we performed an ONC in adult *Tg(gap43:mGreenLantern-CAAX)* fish then carried out longitudinal imaging on the same fish. We observed an upregulation of *gap43* reporter signal in the contralateral optic tectum (cTeO) starting at 4 dpONC, followed by its downregulation by 9 dpONC (**Extended Data 5A-G**). Interestingly, when animals were subjected to an ONT, there was no significant

difference in the *gap43* reporter signal intensity between pre ONT and 5 dpONT in the cTeO (**Extended Data 5H-K**). This suggests that a more severe transection injury does not lead to the appearance of regenerating neurites and corroborates our observation that animals receiving an ONT lack vision recovery when assessed using the DLR assay (**Extended Data 2**). We originally generated the *Tg(gap43:mGreenLantern-CAAX)* transgenic line in *WT* DC. The presence of melanophore pigment cells in the epidermal layer dorsal to the brain (**Extended Data 5D – white arrowheads**), dynamically changed their shape and hindered our ability to quantify and compare the intensity of the *gap43* reporter signal in the same animal's brain over time. To overcome this, we generated a DC pigmentation mutant for *in vivo* imaging of neuro-regeneration. Mutating the *mitfa* gene in zebrafish produced fish that lack melanophores[37]. We identified the DC *mitf* gene using the NCBI DC Genome assembly ASM722483v1, then designed gRNAs to generate a *mitf*$^{-/-}$ mutant line using CRISPR-Cas9 mediated mutagenesis (**Extended Data 6A**). *mitf*$^{-/-}$ mutant DC have reduced melanophore pigment cells when compared to *wild-type* fish, both at larval (**Extended Data 6B-C)** and adult stages (**Extended Data 6E-I**). There was no significant difference in the looming response between *mitf*$^{-/-}$ and *wild-type* animals, suggesting that *mitf*$^{-/-}$ fish have normal vision (**Extended Data 6J**). We performed an ONC on *mitf*$^{-/-}$ animals and assessed their ability to regenerate using the DLR assay. Results between *WT* and *mitf*$^{-/-}$ animals were similar (**Extended Data 6K**). One difference we did observe, however, was that *mitf*$^{-/-}$ animals displayed a significantly slower swim speed in response to a looming stimulus when compared to *wild*-type animals (**Extended Data 6L**).

Pigment-deficient *mitf*$^{-/-}$ fish were used to generate a *Tg(gap43:mGreenLantern-CAAX)* transgenic line. These fish were subjected to ONC and imaged over the course of 10 days. The lack of pigment in this transgenic line allowed us to observe *gap43* reporter signal without melanophore cell obstruction (**Fig. 3A-I**). Growth cones of RGC axons were observed in the cTeO at 4 dpONC (**Fig. 3H-H' and Suppl. Video 4**). Quantification of the *gap43* reporter signal in single z-plane images from the medial TeO zone (**Fig. 3A, 3B'-G'**) showed that *gap43* reporter signal increased in the cTeO at 4 dpONC, peaked at 5 dpONC, then diminished by 8-10 dpONC (**Fig. 3J-K**). No significant difference in the *gap43* reporter signal was observed between males and females at any time-point tested (**Fig. 3K**). In addition, we observed a progression of the *gap43* reporter signal in the cTeO from a rostral to caudal position over time (**3J and 3L and Suppl. Video 4**). While the downregulation of *gap43* reporter signal correlated with results from the DLR assay which showed vision recovery from 5-10 dpONC, the head tilt angle continued to improve after the complete downregulation of *gap43* reporter signal expression (**Extended Data 5L**). We speculate that after *gap43* reporter downregulation, additional modifications occur in the neuronal circuitry facilitating functional recovery. There was no significant upregulation of *gap43* reporter signal in the ipsilateral optic tectum (iTeO) between preONC and 5 dpONC conditions (**Fig. 3M-Q**), suggesting a complete decussation of the optic nerve at the optic chiasm similar to that in zebrafish[25]. Taken together, we have generated a novel DC transgenic line that takes advantage of the *gap43* promoter to visualize *in vivo* axon regeneration. When combined with functional assays, this line has allowed us to correlate cellular phenotypes associated with long distance RGC axon regeneration with vision recovery.

Regenerated axons display an altered topography post ONC. In pro-regenerative vertebrates, studies have shown that RGC axons re-innervate the TeO after an optic nerve injury[24, 29, 38]. However, it is unclear if RGC axons re-establish connections for functional vision recovery by replicating their original topography after injury. Imaging the brain of the same animal before and after injury would help answer this question but this has not been feasible using traditional adult animal models. To compare the topographic map of RGC axons in the TeO before injury and post-regeneration, we used sparse labeling to visualize individual cells by mosaically expressing *isl2b:TdTomato-caax* in *mitf*$^{-/-}$ fish. The zebrafish *isl2b* promoter drives transgene expression in healthy RGCs[39]. We imaged the entire contralateral midbrain region of uninjured fish, subjected them to an ONC injury, then imaged them throughout the

regeneration process (**Fig. 4A**). Compared to pre-injury conditions, we observed degeneration of RGC axons at 1 dpONC as indicated by the fragmentation and reduction of the *isl2b*-driven fluorescent signal in the TeO (**Fig. 4B-C and 4B'-C'**). By 5 dpONC, an extensive network of regenerating neurites was observed (**Fig. 4D and 4D'**). Post-regeneration, neuronal remodeling was observed between 5-10 dpONC (**Fig. 4D-E and 4D'-E'**), corresponding to the time when gradual improvements in the DLR were observed (**Fig. 1D**). When detailed optical sectioning of the cTeO was performed in the same animal before and after an ONC, a general similarity in the arborization fields of RGC axons was observed (**Fig. 4F-K, Suppl. Video 5**). Interestingly, axonal re-modeling continued to occur from 25-40 dpONC, a time-point after injured fish exhibit a normal DLR (**Fig. 4L-P and 4O'-P'**). By comparing the topography of RGC neurites before injury and at 40 dpONC, we observed a stark difference in the dorsal cTeO (**Fig. 4Q**). When imaging at a medial level within the TeO, we observed the expanding arborization of regenerating RGC axons from 10-40 dpONC, a period later than that in the dorsal TeO (**Fig. 4L and 4R-U**). Similar to that in the dorsal TeO, the topography of RGC axons in the deeper medial zone of the TeO pre-injury was distinct from that at 40 dpONC (**Fig. 4V**).

Myelinating oligodendrocyte membrane dynamics during RGC axon regeneration in the cTeO. Myelination in the CNS has been well-documented using longitudinal imaging in developing zebrafish larvae, owing to their optical transparency[40-42]. Based on fixed time-point histological data and results from pooled tissue samples, it has been reported that adult zebrafish can restore myelin to full thickness 4 weeks after a CNS injury[43, 44]. To visualize myelinating oligodendrocyte membrane dynamics and analyze the relationship between myelin and regenerating neurites in adult DC *in vivo*, we generated a double transgenic line *Tg(mbpa:TdTomato-CAAX, gap43:mGreenLantern-CAAX)* where both oligodendrocyte membranes and regenerating neurites are fluorescently labeled. After an ONC, we observed a change in the oligodendrocyte membrane reporter morphology in the cTeO before the appearance of regenerating RGC axons (**Fig. 5A-C, 5B'-C' and 5B"-C"**). Changes in myelination continued to progress when regenerating RGC axons reached the cTeO at 5 dpONC (**Fig. 5D, 5D' and 5D"**). At this time-point, we observed that 17% of myelin fragments were in contact with regenerating neurites (**Fig. 5E-H, 5F'-G', and 5F"-G", Suppl. Video 6**) and larger myelin fragments were in closer proximity to the regenerating neurites than smaller fragments (**Fig. 5I, Suppl. Video 6**). At 17-22 dpONC, when *gap43* reporter signal in the cTeO was diminished, we could detect both de-myelinating and re-myelinating processes (**Fig. 5J-M**). Lastly, the myelin patterns of the cTeO and iTeO appeared to be distinct after injury, even at 60 dpONC (**Extended Data 7**).

In conclusion, our work demonstrates that with the development of unique transgenic lines, robust longitudinal imaging techniques, and vision-based behavioral assays, adult DC can be utilized for comprehensive studies that quantify and correlate CNS axon regeneration, myelination, and functional recovery.

Discussion

Many questions remain unanswered regarding the regeneration of axons in the CNS[45]. A major hurdle has been understanding how regenerating axons re-innervate their targets in the process of reforming functional circuits. Observing this phenomenon *in vivo* and identifying contributing cellular interactions is essential. Some progress has been achieved by comparing the differential regenerative capacity of teleost fish such as zebrafish and medaka[46-49]. However, a limitation to this approach is the inability to analyze the contribution of dynamic spatio-temporal interactions between different cell types during CNS regeneration and functional recovery. In this study, we have established a new adult animal model, *Danionella cerebrum*, for the longitudinal study of CNS regeneration. Harnessing the properties of optical transparency and small size in adulthood, we performed longitudinal *in vivo* imaging of RGC axons and myelin throughout the injury and regeneration process. This approach allowed us

to precisely correlate the cellular events that occur during long-distance axon regeneration with functional recovery.

To obtain a functional reconnection after injury, axons from damaged neurons need to reproduce their pre-injury topography for proper target re-innervation[50, 51]. Classically, the topography of RGC innervation is defined by the retinotectal circuitry map defined by carrying out electrophysiological recordings from populations of axons at different locations within the TeO[52, 53]. Since traditional animal models provide limited *in vivo* optical access to monitor regenerating axons in mature brains, little data is available to determine if axonal innervation topography is important for vision recovery. We tested the hypothesis that vision recovery relies on the post-injury topographical map, produced by regenerated axons, matching its pre-injury state. We performed longitudinal imaging on animals displaying mosaic RGC labeling, monitored progression of regenerating axons after injury, and compared topographies between pre- and post-injury states. After ONC, we observed Wallerian degeneration followed by re-innervation of axons into the cTeO. Initially, regenerating axons formed an extensive network that appeared to follow tracks of degenerating myelin. Later, at a phase coinciding with vision recovery, axon remodeling occurred. Intriguingly, when comparing the topography of axon innervation in the same animal between the pre-injury state and during the remodeling phase, we observed distinct patterns. Our work shows that the DC model, combined with our transgenic lines and imaging methods, provides a powerful platform for the *in vivo* investigation of mechanisms that regulate axonal topography and its refinement.

Insufficient clearance of myelin debris after acute CNS injury is suspected to contribute to the failure of axon regeneration[54]. Our observation that RGC axons can regenerate alongside degenerating myelin suggests that myelin debris may not be a direct hindrance to axonal regeneration in DC. Further investigation is needed to determine the source and nature of different guidance cues involved in the formation of the regenerated RGC axon topography and their role in facilitating functional recovery. Additionally, our imaging revealed that remyelination continued to occur post vision recovery, and that injured animals continued to display reduced myelin levels in the cTeO, suggesting that although functional recovery occurs relatively quickly, return to pre-injury myelin status takes longer or is never achieved.

There are, however, limitations to the current study. We used a sparse labeling technique to demonstrate that RGC axons can regenerate and re-innervate correct targets in the TeO, leading to vision recovery. It remains unclear if all RGCs have the same capacity for axon regeneration. Studies using this sparse labeling approach in combination with specific promoters for RGC subpopulations will provide information on the capacity and necessity for different RGC subpopulations to regenerate in response to guidance molecules. Furthermore, although the DLR and LR assays provide information on the intactness of the animal's vision, visual acuity remains untested. While our results suggest that vision recovery occurs before the completion of remyelination, the relationship between visual acuity and remyelination requires further investigation.

In conclusion, we have shown that using DC to study CNS regeneration *in vivo* represents a powerful and unique opportunity to increase our knowledge of how the nervous system is successfully rewired post injury and gain insight into how this process is regulated.

Materials and Methods

Fish husbandry and maintenance

Danionella cerebrum (DC) were maintained at 28 °C on a 14-10 hour light-dark cycle. Embryos were co-cultured with euryhaline rotifers (*Brachonius plicatilis*) at 5-11 days post fertilization (dpf). At 14 dpf, they were placed into a re-circulating water system and fed rotifers once a day and *Artemia nauplii* twice a day. Fish >1-month post fertilization (mpf) were considered adults and were fed with freshly hatched *Artemia nauplii* twice a day. Spawning was

encouraged by placing a ~6 cm white opaque silicone tube (6 mm ID x 8 mm OD; McMaster-Carr, cat. no. 5054K812) on the bottom of tanks. After collection of embryos, the media in the plate was exchanged every 24 h with E3 containing 10 mM HEPES (Gold Biotechnology, cat. no. H-400-250). All animal work was carried out in accordance with the NIH Guide for Care and Use of Experimental Animals and approved by Medical College of Wisconsin's Institutional Animal Care and Use Committee protocol #AUA00007421.

Generation of expression plasmids and transgenic lines

Tol2-*gap43:mGreenLantern-CAAX* was made by performing a Multisite Gateway LR reaction to assemble the following elements using LR Clonase II Plus enzyme (Thermo Fisher Scientific, cat. no. 12538120): *p5E-gap43, pME-mGreenLantern*, *p3E-CAAX(tH)* (Addgene #109539)[55], and *pDestTol2pA2*[56]. *p5E-gap43* was created by amplifying the *gap43* promoter from plasmid *pW1GFG43SA*[26](a kind gift from Dr. Ava Udvadia), using a polymerase chain reaction (PCR) with the following primers: Forward (F): ggggacaactttgtatagaaaagttggtcgactgtgtggcttccg, and Reverse (R): ggggactgcttttttgtacaaacttgggttcaagttggttctatcctccct. The resulting PCR fragment containing 3624 base pairs of the promoter, the transcription start site, and the 5'UTR sequence stopping immediately before the initial ATG codon was integrated into the pDONR^{TM}P4-P1R vector using a Gateway BP reaction. *pME-mGreenLantern-CAAX* was created by amplifying *mGreenLantern* using *LifeAct-mGreenLantern* (Addgene #164459)[57] as a template and primers F: ggggacaagtttgtacaaaaaagcaggctccaccatggtgagcaagggcgaggagctg,
and R: ggggaccactttgtacaagaaagctgggtgcttgtacagctcgtccatgtcatg. The PCR product was then cloned into *pDONR221* using a Gateway BP reaction. The *Tol2-mbpa:TdTomato-CAAX* and *Tol2-isl2b:Tdtomato-CAAX* expression constructs were created using Gateway LR reactions and combining either *p5E-mbpa* or *p5E-isl2b*[39] with *pME-TdTomato-CAAX* (Addegene #135204)[58], *p3E-polyA* (Tol2kit #302)[56] and *pDestTol2pA2*[56]. The zebrafish *mbpa* promoter[59, 60] was amplified from genomic DNA using primers F: ggggacaactttgtatagaaaagttggcttacactcactgacaaatag and R: ggggactgcttttttgtacaaacttgtctaggtgttgatctgttcag, then integrated into the *pDONR^{TM}P4-P1R* vector using a Gateway BP reaction to create *p5E-mbpa*.

All single transgenic lines and sparsely labeled fish were generated by microinjecting 2-3 nL of a DNA-transposase mixture into 1-4 cell stage *wild-type* (*WT*) DC embryos. The DNA-transposase mixture contained between 8-8.8 ng/µl of DNA, 12.6 ng/µl *in-vitro* transcribed Tol2 transposase mRNA (mMESSAGE mMACHINE™ SP6 Transcription Kit, ThermoFisher Scientific, cat. no. AM1340) and 0.05% phenol red (Sigma, cat. no. P0290) as an indicator. Injected larvae were screened at 4 dpf and animals positive for reporter expression were raised to adults. To generate stable transgenic lines, adult F0 fish were in-crossed to produce F1 embryos that were screened for correct and complete transgene expression. Double transgenic lines were generated by outcrossing fish of the opposite sex from each transgenic line.

Generation of mitf$^{-/-}$ mutant line

Target sites for CRISPR/Cas9-directed mutagenesis were selected with the help of the online tool CHOPCHOP[61-63]. A *mitf* gRNA (5'- GGGAGCCAAACTCAGCCCTC -3') targeting exon 5 of the DC *mitf* gene was used to generate the *mitf* knockout. The generation of the sgRNA template and its subsequent transcription followed previously published protocols (Parvez *et al.,* 2021)[64]. Briefly, the DNA template for *in vitro* transcription was generated using a fill-in reaction of two annealed oligos. One oligo contained the *mitf* targeting sequence along with the SP6 promoter sequence (underlined) ATTTAGGTGACACTATAGGGAGCCAAACTCAGCCCTCGTTTTAGAGCTAGAAAT AGCAAG. The second oligo contained the constant region AAAAGCACCGACTCGGTGCCACTTTTTCAAGTTGATAACGGACTAGCCTTATTTTAACTT GCTATTTCTAGCTCTAAAAC. The fill-in reaction used the following parameters: 98 °C - 2

min, 50 °C - 10 min, 72 °C - 10 min, 4 °C - Hold. The annealed and filled-in oligo was purified using a Zymo DNA Clean and Concentrator-5 kit (Zymo Research, cat. no. D4013). *In vitro* transcription was performed using MEGAscript™ SP6 Transcription kit (ThermoFisher Scientific, cat. no. AM1330) according to manufacturer's guidelines. Samples were then purified using an RNA Clean and Concentrator-5 (Zymo Research, cat. no. R1013). A 5 µl injection mixture was prepared with Buffer 3.1, 1000 ng gRNA, 0.84 µl EnGen Cas9 (NEB, cat no. M0646T). Then, 0.5 nl of the injection mixture was injected into 1-2 cell stage embryos. Genotyping of crispants, wild-type controls, and putative *mitf*$^{-/-}$ F1 animals was carried out by first extracting genomic DNA from tail fin clips (for adults) or from cells isolated by using a Zebrafish Embryo Genotyper (ZEG)[65] (for larvae). PCR primers CCCACATGCCTAAACTTTGCAC and GTTGAGGGTGAGAAGGGCCA flanking the gRNA targeted site were used for PCR amplification of genomic DNA using Phire tissue direct PCR master mix (Thermo Fisher Scientific, cat. no. F170S). PCR products were then purified and sequenced.

Optic Nerve Crush (ONC) and Optic Nerve Transection (ONT)

Adult DC were anaesthetized using 52.24 µg/mL Tricaine-S diluted in fish system water. The fish was positioned on a custom 3-D printed holder at an oblique angle with the eye to be injured facing up. Excess fish water was removed. Under a dissecting microscope with bottom illumination, the optic nerve was exposed by gently removing the connective tissue on the dorsal half of the eye and rotating the eye out of its socket. Using a #5 forceps (Electron Microscopy Sciences, cat. no. 0203-5-PS-1), ONC was carried out by closing the forceps on the optic nerve gently for 5 s while avoiding the ophthalmic artery posterior to the optic nerve. Similarly, ONT was carried out by cutting the optic nerve using micro-scissors (Fine Science Tools, cat. no. 15000-08). Immediately after the procedure, the ONC/ONT site was assessed under a dissecting microscope. A successful ONC was determined if the crushed site became opaque and the axonal tissue remained attached. A successful ONT was determined if the optic nerve head was fully detached from the rest of the optic nerve. The fish were then placed in a recovery tank for approximately 15 minutes or until the fish resumed normal swimming, after which they were transferred to the circulating tank system in the fish facility.

Looming Response (LR) assay

To analyze the recovery of vision in adult DC post optic nerve injury, we adapted an LR assay, that was previously established in zebrafish to assess looming visual stimulus-evoked escape responses[32, 66]. The LR assay was performed in a blackout box measuring 45 cm x 38 cm x 30 cm. The box had a hinged front door and was lit with a uniform white LED light source (Amazon, NXENTC A4 Tracing Light Pad, ASIN: B07D57F8X7) set to maximum brightness (1630 lux) to provide contrast for recording and tracking of fish. The fish was placed in a clear plastic tank (Michaels, cat. no. 10728059) measuring 10.16 cm x 20.32cm x 7.62 cm and filled with 770 mL of fish water maintained at 24-28 °C. The bottom and lateral insides of the tank were covered in matte-clear tape (Amazon, Gaffer Power Transparent Duct Tape, ASIN: B076J2BS1B) to reduce internal reflection. The tank was placed in the blackout box 2.9 cm away from the LED light screen. The camera (Logitech, P/N: 860-000451, 1080p, 30fps) was placed 33 cm from the light screen to capture images of the whole tank. A Raspberry Pi monitor, 15x23.5 cm, (Amazon, ROADOM Raspberry Pi Screen, ASIN: B09XDK2FRR), mirrored a computer monitor that played the stimulus video. The monitor was centered and placed face down at 2.54 cm above the water. The stimulus video was created using Adobe Premiere Pro 2024 (Version 24.0.1). The video projected a white screen for 2 min, followed by a looming stimulus presented as an expanding circle. The opacity, expansion speed and final size of the circle were optimized to illicit a robust change in swimming speed of uninjured *WT* fish while the stimulus appeared. An expanding opaque black circle that grew from 0 to 10.8 cm at a radius growth rate of 5.4 cm/s was used. The opaque black circle expanded over 2 s and remained on the screen for one minute. As the stimulus appeared, a grey rectangle appeared on the right side of the screen to allow for accurate tracking of the stimulus during

analysis. This grey rectangle was reflected to the camera by a mirror (Amazon, Iconikal Metal Compact, ASIN: B0B75R1K8N) placed beside the tank.
Fish can respond to a looming stimulus even with one functional eye. To accurately assess the time-course of vision recovery post ONC, an ONT was first performed on the left eye of the fish to induce permanent blindness, followed by an ONC on the right eye of the same fish one day later. A LR assay was performed on the same fish over the course of 12 days to assess the recovery of vision on the ONC-injured eye. The fish was given adequate time (5-20 min) to acclimate to the looming tank environment before the looming assay was performed. Acclimation was considered complete when the fish displayed leisurely swimming throughout tank.
An ANY-Maze video tracking system (Stoelting Co., Version 7.4) was used for animal tracking. A Python code was created to analyze the data generated from ANY-Maze. The code identified the exact time the visual stimulus appeared by detecting the change in pixel intensity in the reflection of the mirror. The code averaged the swim speed of the fish 1 s before the stimulus and 1 s as the stimulus was played. Two trials were conducted per fish for each time-point. Fish showed minimal looming responses at 1-day post ONC (dpONC). The average change in speed at this time-point was used as the baseline for determining a reaction score. If a trial's average change in speed was greater than one standard deviation of the average change in speed at 1 dpONC, the trial scored a 1 and considered a positive response, otherwise, the trial scored a 0 and was considered a non-response. The score was averaged for the two trials at each time-point for each fish. The scores were converted to a percentage and graphed using GraphPad Prism (Version 10.4.1).

Dorsal light response (DLR) assay
The Dorsal Light Response (DLR) assay[27, 28, 30, 31] was adapted for DC and used to investigate the behavioral response of fish to visual stimuli by quantifying the tilt angle of the head orientation while swimming. Single fish were acclimated for 5 to 10 minutes (until normal swim behavior was observed) in a clear acrylic chamber (6 cm x 6 cm x 6 cm) containing 130 mL of fish water maintained at 24-26 °C. Each apparatus had two side-by-side chambers, allowing for simultaneous recording of two fish. The lateral and bottom insides of the chamber were lined with 100% light blocking white vinyl (Amazon, VELIMAX White Blackout Window Film, ASIN: B08P8KQCL4), while the front was covered with one-way mirror film (Amazon, KESPEN Window Privacy Film One Way, ASIN: B07PBTWCXC) with 28% visible light transmission, oriented such that the reflective side faced inward. The back side of the chamber remained transparent. A uniform white LED light source (Invitrogen, cat. no. LB0100) illuminated the chamber from the back, operating at its maximum light intensity (17900 lux) setting to provide optimal contrast for video capture.
Fish were filmed swimming toward the mirror film using a camera (iPhone 11, 1080p resolution, 30 fps) positioned 12.5 cm away from the front of the chamber. The camera was focused on the center of the chamber, with fish monitored during recording to ensure head-on views were captured. Video recordings varied in length from less than 1 min to approximately 5 min. For analysis, 3-5 frames were captured from each video recording, where the fish was positioned head-on relative to the camera. Head tilt angles were measured from the captured frames using Fiji[67]. Specifically, the straight-line tool was used to draw a line connecting the top pixel of one eye to the top pixel of the other eye. This line was aligned at the intersection of a cross to facilitate the angle measurement. The angle was quantified using the angle tool in Fiji. The change in head tilt angle was normalized by subtracting the head tilt angle at pre-ONC time-point to each time-point. Fish possessing a change in head tilt angle above 10 degrees at 1 dpONC were considered for further analysis. The change in head tilt angle was measured over several days and plotted using GraphPad Prism (Version 10.4.1).

Fish mounting and intubation for imaging
For larval DC: At the desired developmental stage, larval DC were anaesthetized using 200 µg/mL Tricaine-S (Fischer Scientific, cat. no. NC0342409) diluted in E3 containing 10 mM HEPES (GoldBio, cat. no. H-400-500). Anaesthetized larvae were mounted for imaging using

1% low melt agarose (Apex Bioresearch, cat. no. 20-104) in E3 in the desired orientation on a 3.5 cm glass bottom petri dish (Cellvis, cat. No. D35-20-0-N). Once the agarose had hardened, 2 mL of 200 µg/mL Tricaine-S in E3 was added to the petri dish to cover the agarose.
For adult DC: Fish were lightly anaesthetized with 65 µg/mL Tricaine-S diluted in fish water and then embedded in 4% low melt agarose (Apex Bioreserach, cat. no. 20-104) dissolved in E3 buffered with 10mM HEPES on a custom imaging chamber equipped with an intubation inflow tube that was placed inside the mouth of the fish, supplying fresh fish water for the duration of imaging, as previously described[10]. For long-term time-lapse imaging of regeneration, fish were mounted and then intubated with 65 µg/mL Tricaine-S diluted in fish water for the duration of imaging.

Image acquisition
All images were acquired using the NIS elements (Version 5.41.01) software on a Nikon Ti2 inverted microscope fitted with a Yokogawa CSU-W1 spinning disk confocal head. Images were captured using a Prime 95B Scientific CMOS camera, and fluorophores were excited using a 488 nm or 561 nm excitation laser. Images were captured using the following objectives: 4× Air 0.2 N.A., 10× Air 0.45 N.A., 20× Air 0.75 N.A. or 40× Water 1.25 N.A.

Analysis of gap43 reporter signal
All quantification was performed using Fiji and graphs were generated using GraphPad Prism (Version 10.4.1). For the analysis of developmental downregulation of *gap43* reporter signal in **Suppl. Fig. 4**, *gap43* reporter signal was quantified using maximum intensity projection (MIP) images from confocal z-stack images. A fixed region of interest (ROI) was defined in the hindbrain, midbrain, and forebrain using the bright-field image as guidance (ROIs marked in **Suppl. Fig. 4**). Mean signal intensity in the ROI was calculated and normalized to 2-months post fertilization (mpf) using the formula: mean intensity in the ROI at X mpf time-point /2 mpf time-point. For the analysis of *gap43* reporter signal in response to an optic nerve injury in **Fig. 3K, 3Q** and **Suppl. Fig. 5H, 5L**, *gap43* reporter signal was quantified using single z-plane images at the medial contralateral optic tectum (cTeO; ROI as shown by the white dotted line in **Fig. 3B'-G', B''-G''** and yellow dotted line in **O-P**). The mean intensity under the line-ROI indicated in **Fig. 3J** was calculated at different time-points and normalized with pre ONC using the formula: mean intensity the under the line-ROI at X dpONC time-point/ pre ONC. For the analysis of *gap43* reporter signal in different TeO regions in **Fig. 3L**, the intensity of *gap43* reporter signal under the line-ROI from the rostral to caudal cTeO was plotted.

3-D analysis of myelin and regenerating neurites
Imaris (Version 10.1.1) was used to carry out 3-D quantification of myelin fragments with respect to regenerating neurites. First, surface segmentation of the regenerating neurites was created by training the machine learning (ML) algorithm through the steps of defining fluorescent signal as "foreground" and background signal as "background" with the "object-object statistics" settings set to "on." When the "foreground" and "background" matched the corresponding signal, ML training was considered complete. ML was applied to generate surface segmentation of regenerating neurites. Next, each surface rendering was subjected to thresholding with a minimum volume of 100 μm^3. Surface segmentation of auto-fluorescent signal was then manually removed. Lastly, all regenerating neurite surfaces were unified as a single surface.
The surface segmentation for the myelin was created by using ML. After which, surface segmentation of myelin fragments was refined by manual editing. Since the myelin reporter construct drives membrane targeting of fluorescent proteins in oligodendrocytes, we removed surface segmentation of oligodendrocyte cell bodies to ensure that the analysis was only performed with respect to myelin fragments. After surface segmentation, statistics of the "volume" for each myelin fragment and the shortest distance of each myelin fragment to the surface of regenerating neurites was exported. For **Fig. 5H**, any myelin fragment that was at 0 µm distance from the regenerating neurites was considered "in contact" with regenerating

neurites. For **Fig. 5I**, the range of distances between myelin fragments and regenerating neurites was plotted against the volume of each myelin fragment. All plots were created using GraphPad Prism (Version 10.4.1).

Post-acquisition image processing and video rendering

Post-acquisition, images in **Fig. 3H-I,** and **Figs. 4-5** were subjected to Denoise.ai (NIS elements Version 5.41.01). For image registration across different time-points, an image from the brightfield channel was used as a reference. Images in **Figs. 3-5** were registered in the X-Y direction using the "Align Image by Line ROI"[68] Fiji plug-in. Additionally, in **Fig. 4B-E, 4B'-E'** and **4M-V**, the "BigWarp"[69] Fiji plug-in was used for 3-D image alignment. In **Suppl. Video 4**, video alignment was done using the FiJi plug-in "Linear Stack Alignment with SIFT"[70]. In **Suppl. Video 5** and **6**, Denoise.ai (NIS elements Version 5.41.01) and 3-D deconvolution (NIS elements Version 5.41.01; parameters used were: "Deconvolution Method" : Automatic, "Modality" : Spinning Disk, "Pinhole Size": 50.00 µm, "Magnification" : 40.0x, "Numerical Aperture" : 1.15, "Immersion Ref. Index" : 1.333, "Calibration" : 0.275 µm/px, "Z-step" : 0.400 µm) were applied. 3-D rendering videos were created using the "Movie Maker" function in NIS elements. Adobe Premiere Pro (Version 24.1.0) was used to add titles, annotations, timestamps, and to sync videos.

Statistical analysis

Preliminary n number estimations were done using G*power[71] (Version 3.1.9.4; $\alpha = 0.05$, and power $(1-\beta) = 0.95$). All statistical analysis post data acquisition was performed using GraphPad Prism (Version 10.4.1). All data were tested for normal distribution using the Kolmogorov–Smirnov normality test. 2-Tailed Unpaired t-tests were performed when means of 2 unrelated groups were compared. A Kruskal-Wallis Test was carried out with non-normally distributed data when means of more than 2 unrelated groups were compared. A Repeated Measures 1-way ANOVA was carried out when means of 1 group of fish were compared over time. A Repeated Measures 2-way ANOVA was carried out when means of 2 or more groups of fish were compared over time. The mixed effects ANOVA model was fitted when the sample size of each group was different.

Acknowledgements

Ross Collery cloned the *pME-mGreenLantern* construct. Hannah G. Tebbs performed the LR reaction and purified the *gap43:mGreenLantern-CAAX* construct. This work is funded by the National Institutes of Health Office of the Director under Award Number R21OD033664 (P.Y.L.), S10OD032136 (to Brandon Tefft - MCW engineering core), and the Advancing a Healthier Wisconsin Endowment (P.Y.L). Portions of the schematic diagrams were created using BioRender (BioRender.com).

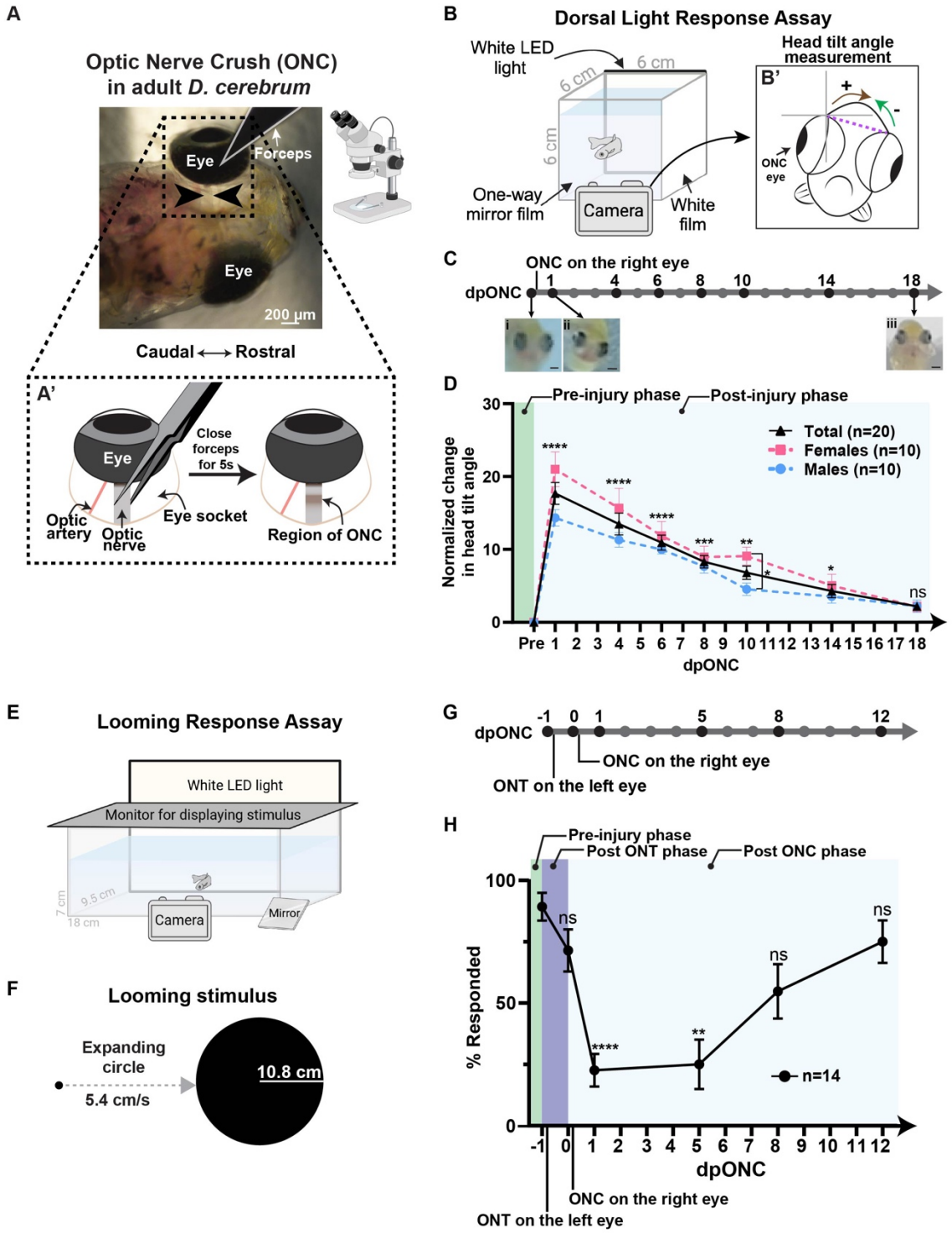

Figure 1. Assessing functional recovery after an optic nerve crush (ONC) using Dorsal Light Response (DLR) and Looming Response (LR) Assays. (A) Dorsal view of an adult DC pre ONC with black arrowheads flanking the optic nerve. **(A')** Schematic representation of the black dotted area in (A) illustrating the ONC procedure. After a successful ONC, the region of the optic nerve subjected to ONC turns opaque. **(B)** Schematic representation the DLR assay chamber. **(B')** Illustration of how the head tilt angle is measured. Brown arrow showing a right tilt (positive angle) and green arrow showing a left tilt (negative angle). **(C)** Timeline schematic of the DLR assay with the time-points that head tilt angle was measured indicated by black dots. (i-iii) Representative images of the same fish (i) pre ONC, and at (ii) 1-day post

ONC (dpONC) and (iii) 18 dpONC. Scale bar = 200 μm. **(D)** Change in head tilt angle compared to Pre-ONC values. All data are represented in mean ±SEM. Black solid line represents all animals (n = 20), pink dotted line represents females (n = 10), and blue dotted line represents males (n = 10). *P* values were calculated using Repeated Measures 2-way ANOVA. *P* values of all animals (total) of each time-points are indicated above the trace where pre and post ONC measurements were compared. *P* values from left to right: $P = <0.0001$, $P = <0.0001$, $P = <0.0001$, $P = 0.0001$, $P = 0.0042$, $P = 0.0189$, and $P = 0.1237$. For females vs males, at 1 dpONC, $P = 0.0619$; at 4 dpONC, $P = 0.3286$; at 6 dpONC, P = 0.6492; at 8 dpONC, $P = 0.7341$; at 10 dpONC $P = 0.0195$; at 14 dpONC $P = 0.6938$; and 18 dpONC $P = 0.9994$. ns, $P > 0.1234$; * $P \leq 0.0332$; ** $P \leq 0.0021$; *** $P \leq 0.0002$; and **** $P \leq 0.0001$. **(E)** Schematic representation of the LR Assay. **(F)** Schematic illustration of the expanding circle parameters used in the LR assay. **(G)** Timeline schematic of the LR assay with the time-points that LR was assessed indicated by black dots. **(H)** Percentage of fish responding to the LR stimulus pre and post injury. All data represented in mean ±SEM (n = 14 including 7 females and 7 males). *P* value of each time-point was calculated using Mixed Effects Repeated Measures 2-way ANOVA. *P* values represented as compared to -1 dpONC/pre-injury time-point. *P* values from left to right: $P = 0.6166$, $P = <0.0001$, $P = 0.0046$, $P = 0.2088$, and $P = 0.9610$. ns, $P > 0.1234$; ** $P \leq 0.0021$; and *** $P \leq 0.0002$.

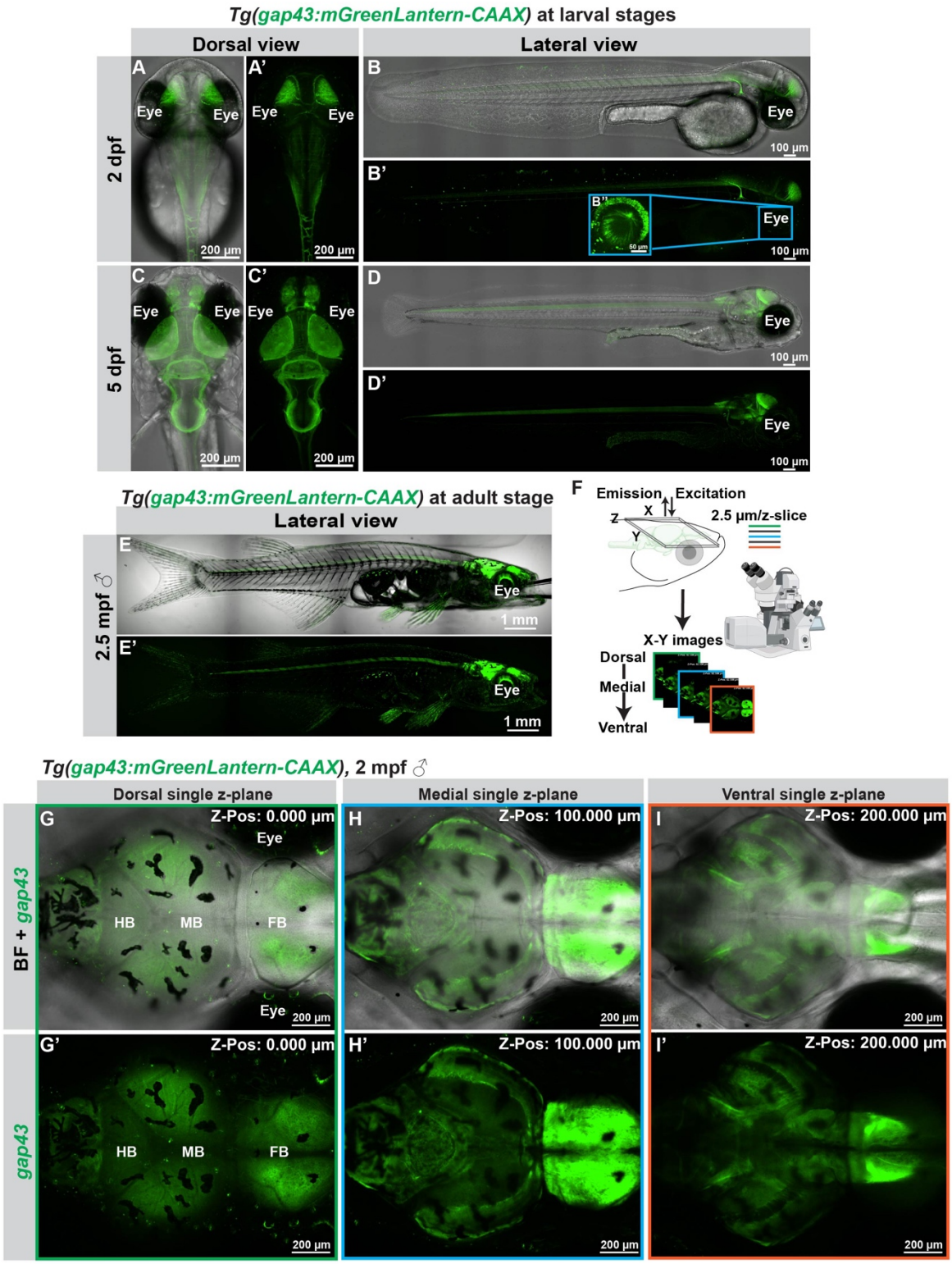

Figure 2. Generating the *Tg(gap43:mGreenLantern-CAAX)* axonogenesis reporter line. **(A-D)** and **(A'-D')** Confocal images of *Tg(gap43:mGreenLantern-CAAX)* larvae acquired using a 20X objective (N.A. = 0.75, 0.9 µm/step). **(A-D)** *gap43* promoter driven expression (green channel) overlayed with the bright field (BF) channel in 2- and 5-days post fertilization (dpf) larvae. **(A-A' and C-C')** Dorsal confocal maximum intensity projection (MIP) images. The total z-stack was 199.80 µm in (A-A') and 246.60 µm in (C-C'). (B-B' and D-D') Lateral confocal MIP images. The total z-stack was 199.90 µm in (B-B') and 199.80 µm in (D-D'). (B'') Inset of the region marked in the blue rectangle in B' showing *gap43*-driven expression of fluorescent protein in the eye. **(E-E')** Lateral confocal MIP images of an adult *Tg(gap43:mGreenLantern-*

CAAX) male at 2.5 months post fertilization (mpf). Image was acquired using a 4X objective (N.A. = 0.2). The total z-stack was 1050 µm with a 25 µm/step. ♂ = Male. **(E)** *gap43* promoter driven expression (green channel) overlayed with the BF channel. **(E')** Green channel only. **(F)** Schematic representation of the approach used to acquire confocal images of the adult DC brain (images shown in G-I and G'-I'). Z-stacks were acquired at 2.5 µm/z-step using a 10X objective (N.A. = 0.45) on a 2 mpf *Tg(gap43:mGreenLantern-CAAX)* male measuring 1.32 cm in length. **(G-I)** *gap43* promoter driven expression (green channel) overlayed with the bright field (BF) channel. **(G'-I')** Green channel only. FB = Forebrain, MB = Midbrain and HB = Hindbrain. **(G and G')** Single plane image of the dorsal brain (z-position= 0.00 µm). **(H-H')** Single plane image of the medial brain (z-position = 100.00 µm). **(I-I')** Single plane image of the ventral brain (z-position = 200.00 µm).

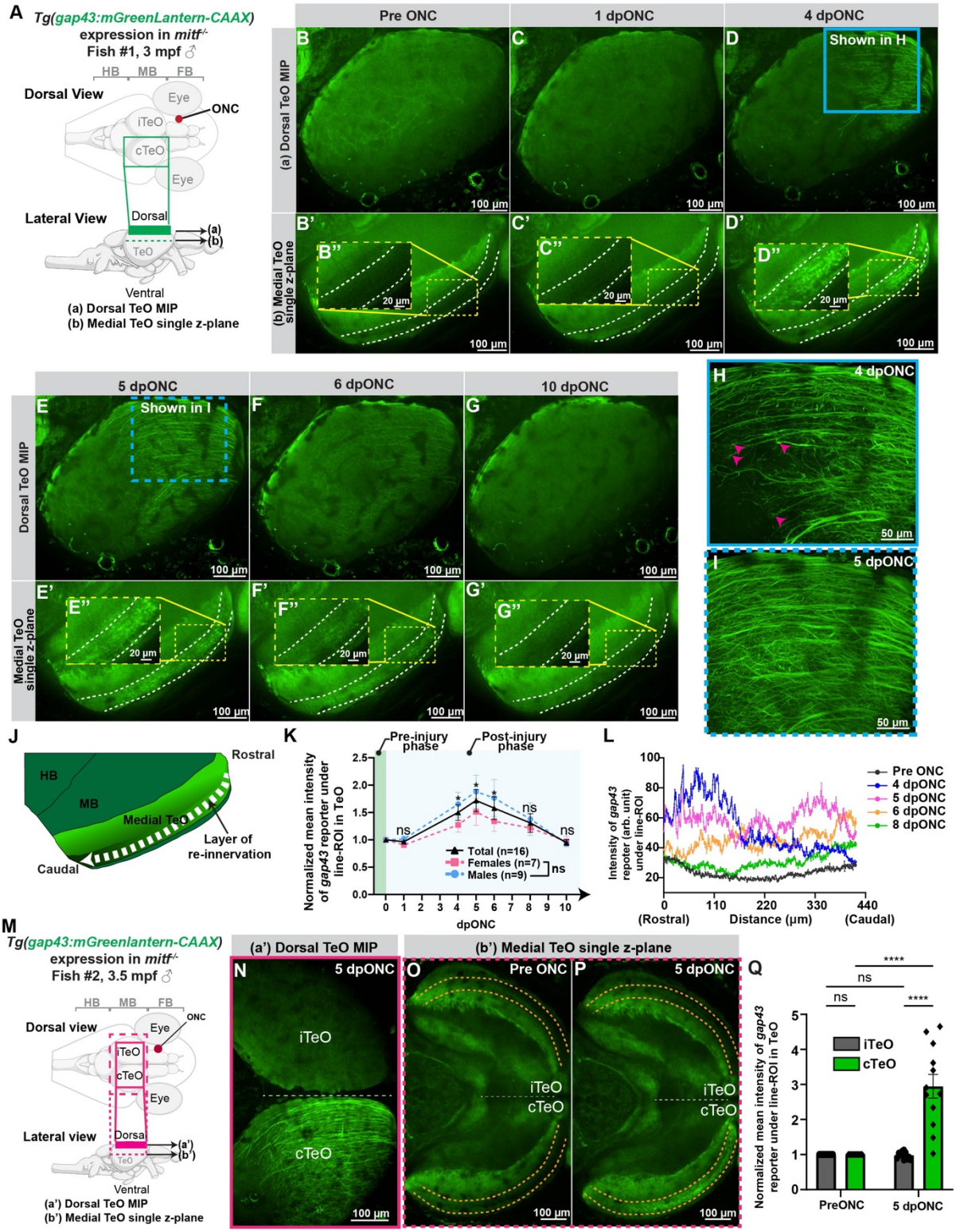

Figure 3. Longitudinal confocal imaging of RGC axon regeneration after an ONC injury. (A) Schematic illustrations showing the imaged area depicted in B-G and B'-G'. The solid green rectangle in the lateral view (a), corresponds to the area imaged and presented as maximum intensity projections (MIPs) of the dorsal portion of the TeO (optic tectum) in B-G. The green dotted line in the lateral view (b), corresponds to an area more ventral to (a) and presented as single plane images of the medial TeO in B'-G'. FB = Forebrain, HB = Hindbrain, MB = Midbrain, cTeO = contralateral TeO and iTeO = ipsilateral TeO and ♂ = Male. **(B-G, B'-G', B"-G")** Confocal images acquired in a *Tg(gap43:mGreenLantern-CAAX)* male *in mitf*$^{-/-}$ at 3-months post fertilization (mpf) with a length of 1.36 cm using a 20X objective (N.A. = 0.75,

0.9 µm/z-step). **(B-G)** Dorsal TeO MIP images of the *gap43* promoter-driven fluorescent signal at the indicated time-points. The total z-stack thickness was 117.00 µm in (B), 115.20 µm in (C), 119.70 µm in (D), 112.50 µm in (E), 115.20 µm in (F), and 118.80 µm in (G). dpONC = days post ONC. **(B'-G')** Single plane images of a deeper (medial) region in the TeO of the same fish. **(B''-G'')** Magnified area corresponding to the yellow dotted rectangle in B'-G'. Measurements of *gap43* reporter signal were made in the region bounded by the white dotted lines. **(H)** Magnified view of the region indicated by a blue rectangle in D (magenta arrows = growth cones). **(I)** Magnified view of the region indicated by a blue rectangle in E. **(J)** *gap43* reporter signal intensity was quantified in the area indicated by the white dotted line. This area represents the site of re-innervation (marked by black arrow). **(K)** Mean intensity of *gap43* reporter expression in the ROI indicated in (J) normalized to pre ONC levels was measured for 10 dpONC. All data represented in mean ±SEM. Black dotted line represents all animals (n = 16), pink dotted line represents the females (n = 7), blue dotted line represents the males (n = 9). *P* values at each time-point compared to pre ONC were calculated using Mixed Effects Repeated Measures 2-way ANOVA. *P* values of all animals (total) from left to right: $P = 0.9728$, $P = 0.0446$, $P = 0.0346$, $P = 0.1417$, $P = 0.5474$, $P = 0.9576$. For females vs males, at 1 dpONC, $P = 0.3399$; at 4 dpONC, $P = 0.3250$; at 5 dpONC, $P = 0.6274$; at 6 dpONC, $P = 0.5323$; at 8 dpONC $P = 0.8613$; and at 10 dpONC $P = 0.9375$. ns, $P > 0.1234$; and * $P \leq 0.0332$. **(L)** Intensity of *gap43* reporter signal (arbitrary units) in the TeO ROI (indicated in J) measured in the same animal at the time-points indicated. **(M)** Schematic representation of regions and depths imaged in N-P. Magenta rectangle in the dorsal view shows the region imaged in (N) and the dotted rectangle shows the region in O-P. (a') Solid bar corresponds to the region imaged and shown in (N) as a MIP. (b') Dotted line corresponds to the single plane images shown in (O-P). **(N-P)** Confocal images acquired using a 10X objective (N.A. = 0.45, 2.5 µm/z-step) in a *mitf*$^{-/-}$ *Tg(gap43:mGreenLantern-CAAX)* male at 3.5 mpf with a length of 1.30 cm. White dotted line separates the cTeO and the iTeO. **(N)** Dorsal TeO MIP image of the expression of *gap43* reporter at 5 dpONC. The total z-stack thickness was 125.00 µm. **(O-P)** Medial TeO single z-plane image of the expression of *gap43* reporter at time-points indicated. The ROI quantified in Q is demarked by the orange dotted lines. **(Q)** Intensity of *gap43* reporter expression normalized to pre ONC levels in the ROI indicated in (O-P). All data represented in mean ±SEM (n = 12). *P* values calculated using Repeated Measures 2-way ANOVA. For pre ONC, iTeO vs cTeO $P = >0.999$; for 5 dpONC, iTeO vs cTeO $P = <0.0001$; for iTeO, pre ONC vs 5 dpONC $P = 0.9349$; for cTeO; and pre ONC vs 5 dp ONC $P = <0.0001$. ns, $P > 0.1234$; and **** $P \leq 0.0001$.

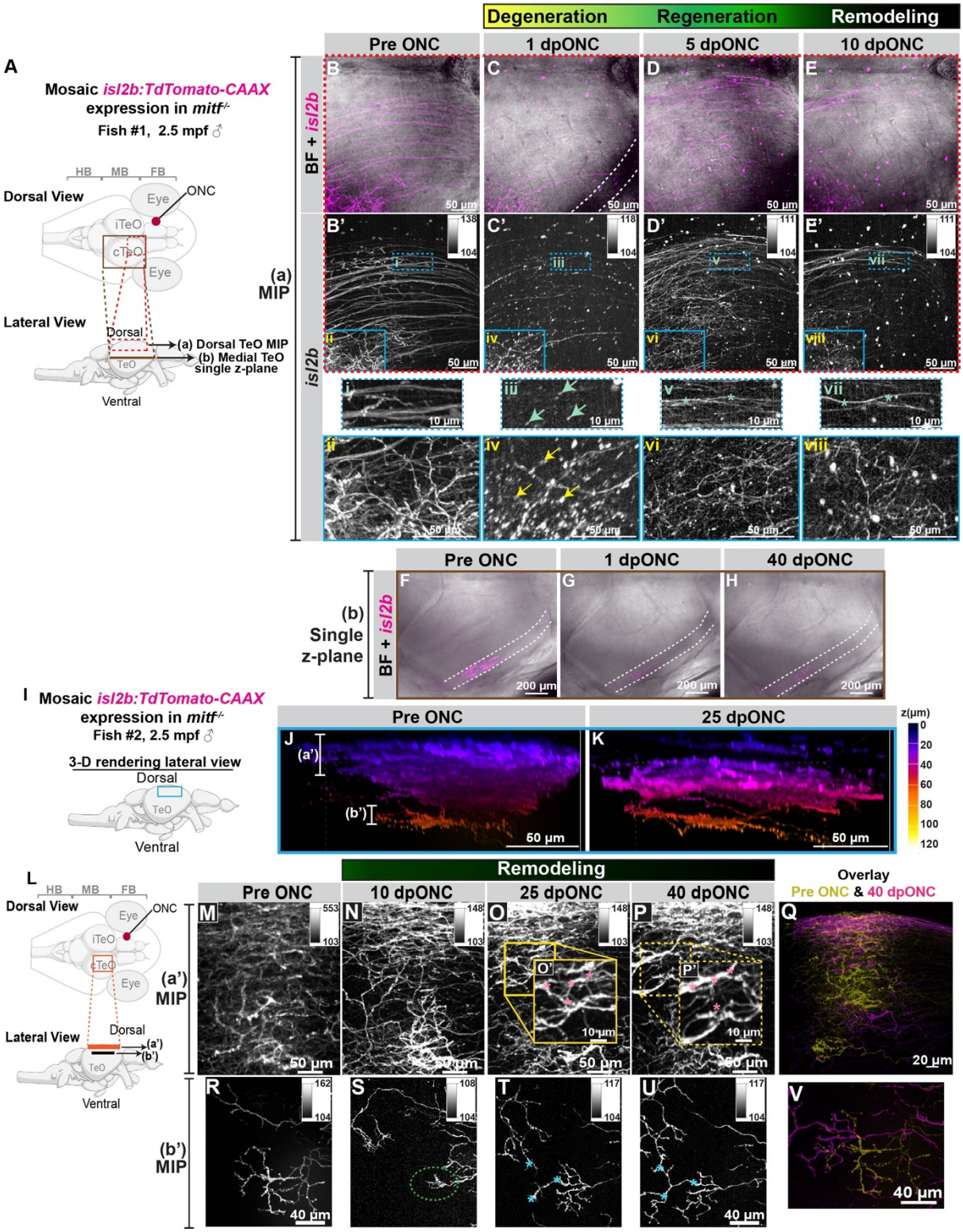

Figure 4. Longitudinal assessment of the topography of RGC axons pre- and post-ONC using sparse labeling. (A) Schematic representation of regions imaged and shown in B-E and B'-E'. (a) Red dotted rectangle corresponds to the dorsal optic tectum (TeO) area imaged and shown as a MIP in B-E and B'-E'. (b) Solid brown line indicates the position within the TeO imaged and shown as a single z-plane image in F-H. FB = Forebrain, MB = Midbrain, HB = Hindbrain, cTeO= contralateral TeO, iTeo= ipsilateral TeO and ♂ = Male. **(B-E)** and **(B'-E')** All images were acquired using a 40X objective (N.A. = 1.15, 0.4 µm/z-step) in a male *mitf*$^{-/-}$ fish at 2.5-months post fertilization (mpf) 1.34 cm in length with mosaic *isl2b:TdTomato-CAAX* expression. The total z-stack thickness used for MIP was 112 µm. **(B-E)** MIP images showing

the mosaic expression of *isl2b:TdTomato-CAAX* (magenta) combined with the corresponding bright field (BF) image in the dorsal region of the TeO at the time-points indicated. Dotted line in (C) indicates the location of the darker shade neuronal debris accumulation in the cTeO at 1-day post ONC (dpONC). **(B'-E')** Grey scale images of B-E with look-up tables (LUTs) shown in the upper right inset. **(i-viii)** Magnified view of regions of interest as indicated by rectangles in B'-E'. Green and yellow arrows highlight degenerating *isl2b:TdTomato-CAAX* expressing neurites. Green asterisks highlight remodeling of *isl2b:TdTomato-CAAX* expressing neurites. **(F-H)** Single z-plane images of medial TeO region showing the mosaic expression of *isl2b:TdTomato-CAAX* (magenta) combined with the corresponding bright field (BF) image at the time-points indicated. Dotted line indicates the area of the TeO where *isl2b:TdTomato-CAAX* expressing neurons are innervating. Images were acquired using a 20X objective lens (N.A. = 0.75). **(I)** Schematic representation of the lateral view of the *D. cerebrum* brain where the blue box represents the region imaged, three-dimensionally (3-D) rendered, and presented in J-K. **(J-V)** Images were acquired using a 40X objective (N.A. = 1.15, 0.4 μm/z-step) in a male *mitf*$^{-/-}$ fish at 2.5 mpf and 1.36 cm in length with mosaic *isl2b:TdTomato-CAAX* expression. **(J-K)** Color coded 3-D rendered images of mosaic *isl2b:TdTomato-CAAX* expression at the time-points indicated. The total z-stack thickness was 125.6 μm and imaging z-depth is indicated in the scale. (a') and (b') Represent the z-depth region shown in the MIP images of (M-Q) and (R-V), respectively. **(L)** Schematic representation of regions imaged and shown in M-V. The orange rectangle (a') indicates the region shown M-Q and the black rectangle (b') indicates the region shown in R-V. **(M-P)** MIPs of the dorsal TeO region before ONC injury and at the time-points indicated. Yellow boxes are magnified ROIs (O' and P'). Pink asterisks = remodeling of *isl2b:TdTomato-CAAX* expressing neurites. **(Q)** Overlay of Pre ONC (yellow) and 40 dpONC (magenta) images. The total z-stack depth was 72.4 μm for M-Q. **(R-U)** MIPs of a deeper medial TeO region before ONC injury and at the time-points indicated. Dotted green oval = re-forming arbor field. Blue asterisks = remodeling of *isl2b:TdTomato-CAAX* expressing neurites. **(V)** Overlay of Pre ONC (yellow) and 40 dpONC (magenta) image. The total z-stack depth was 25.6 μm for R-V.

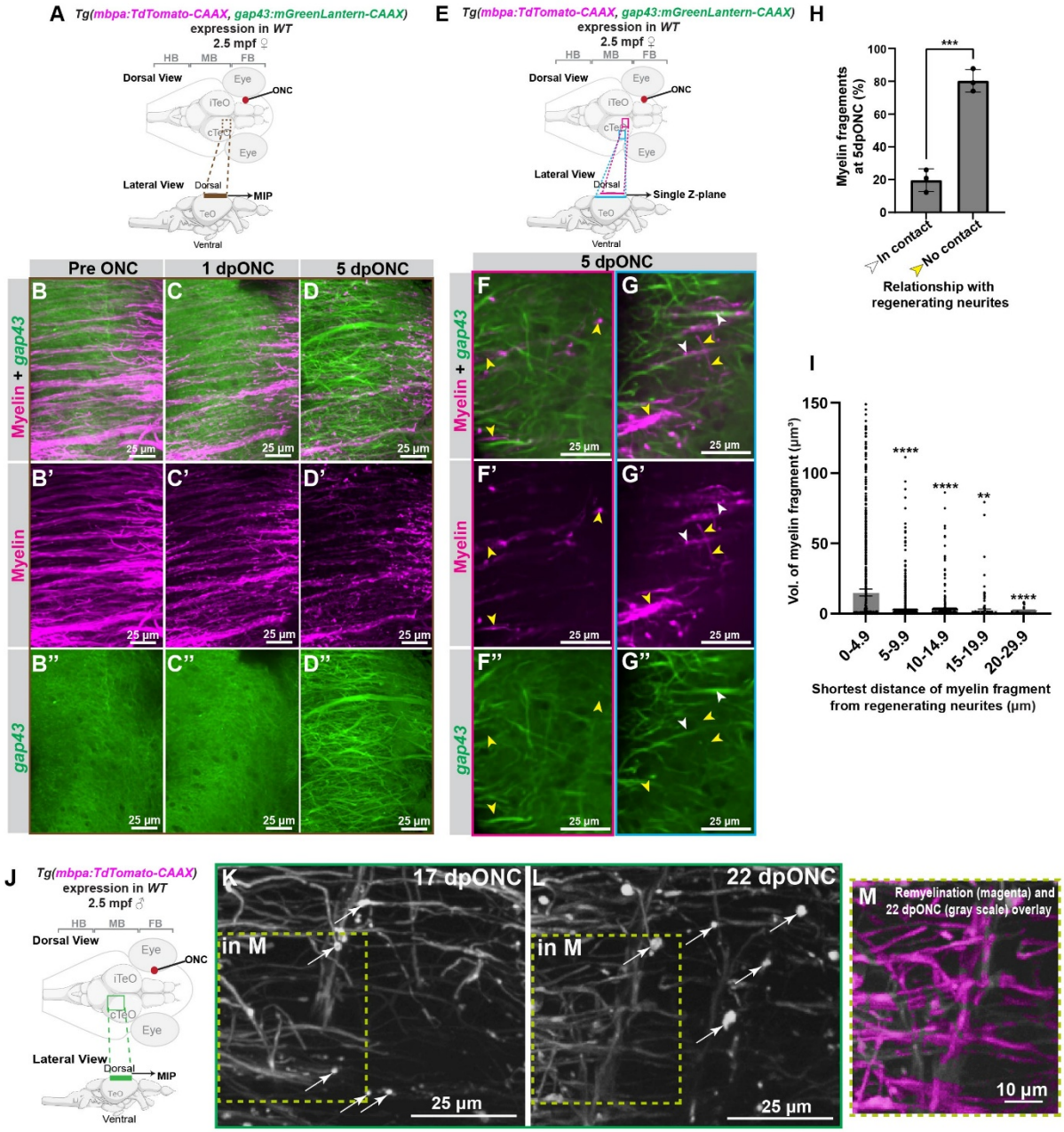

Figure 5. Correlating RGC axonal regeneration with oligodendrocyte membrane reporter expression in the optic tectum (TeO) after an ONC. (A) Schematic representation of area imaged in B-D, B'-D' and B''-D'' is indicated by the brown rectangles in the dorsal and lateral view. Images were acquired then presented as MIPs with a 40X objective (N.A. = 1.15, 0.4 µm/z-step) in a double transgenic female *Tg(mbpa:TdTomato-CAAX, gap43:mGreenLantern-CAAX)* at 2.5-months post fertilization (mpf) and 1.37 cm in length. FB = Forebrain, MB = Midbrain, HB = Hindbrain, cTeO = contralateral TeO, iTeo = ipsilateral TeO and ♀ = female. **(B-D)** Merged fluorescent signals from the myelin reporter (magenta) and the *gap43* reporter (green). **(B'-D')** Myelin reporter (magenta) only. **(B''-D'')** *gap43* reporter (green) only. **(E)** Schematic representation of the regions imaged in F-G, F'-G', and F''-G''. All images are single z-planes in the area and depths indicated. **(F-G)** Merged fluorescent signals from the myelin reporter (magenta) and the *gap43* reporter (green). **(F'-G')** Myelin reporter (magenta) only. **(F''-G'')** *gap43* reporter (green) only. White arrowheads indicate regions of contact between both myelin and *gap43* reporter expression. Yellow arrow heads indicate regions where only myelin reporter expression is seen. **(H)** Percentage of signals from both myelin and *gap43* reporters making contact and not making contact at 5-days post ONC

(dpONC). *P* value was calculated using 2 Tailed Unpaired T-test. *** $P = 0.0004$. **(I)** Volume of myelin signal (μm^3) in relation to the shortest distance to *gap43* reporter signal (µm). *P* value was calculated against 0-4.9 µm using Kruskal-Wallis Test (from right to left: $P = <0.0001$, $P = <0.0001$, $P = <0.0024$, $P = <0.0001$. ** $P \leq 0.0021$ and **** $P \leq 0.0001$. For H-I, all data represented as mean ±SEM. (n = 7529 myelin fragments analyzed in 3 fish in a volume of 100 µm (x), 100 µm (y), 78 µm (z)). **(J)** Schematic representation of the region imaged in a double transgenic male *Tg(mbpa:TdTomato-CAAX, gap43:mGreenLantern-CAAX)* fish, 2.5-months post fertilization (mpf) with a length of 1.27 cm, that was subjected to an ONC injury. Confocal images presented as MIPs in K-L. ♂ = male. **(K-L)** All images were acquired using a 40X objective (N.A. = 1.15, 0.4 µm/z-step). The total z-stack thickness was 33.33 µm. **(K)** Signal from the myelin reporter in the cTeO region at 17 dpONC presented in greyscale. **(L)** The same region from the same fish was imaged at 22 dpONC. (White arrows = myelin fragments). **(M)** Overlay image of remyelination (magenta; fluorescent signal subtraction of area shown in L from K) and 22 dpONC (gray scale).

Extended Data 1. Apparatus for the Dorsal Light Response (DLR) and Looming Response (LR) Assays. (A) The DLR assay uses a 2-chamber (dimensions of 1 chamber = 6 cm x 6 cm x 6 cm) container which was covered by an opaque white film on 3 sides. The back of the DLR chamber facing the white LED light source was transparent. The front of the DLR chamber was covered with a 1-way mirror film. A camera was positioned on a stand in front of the DLR chamber. **(B)** The LR assay was performed in a blackout box with a closeable front door, inside which the LR chamber was positioned with a white LED source in the back. A monitor, used to present the LR stimulus to the fish, was positioned on the top of the LR chamber. A camera was positioned on a stand in front of the LR chamber. A mirror reflecting the presence of the LR stimulus to the camera was positioned on the right of the LR chamber.

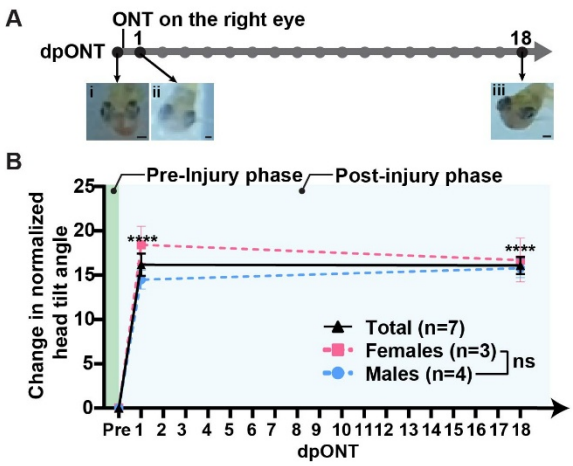

Extended Data 2. Assaying vision recovery after optic nerve transection (ONT) using the Dorsal Light Response (DLR) assay. (A) Schematic of the timeline used for the ONT experiment. The black dots indicate on what days the DLR assay was performed. (i-iii) Representative images of the same fish at (i) Pre ONT, (ii) 1-day post ONT (dpONT) and (iii) 18 dpONT. Scale bar = 200 µm **(B)** The change in head tilt angle, normalized to the pre-ONT angle, was plotted for the days tested. All data represented in mean ±SEM. Black dotted line represents all animals (n = 7), pink dotted line represents the females (n = 3), blue dotted line represents the males (n = 4). *P* value of all animals (total) at each time-point as compared to pre ONT was calculated using Mixed Effects Repeated Measures 2-way ANOVA. *P* values from left to right: $P = <0.0001$, and $P = <0.0001$. For males vs females, at 1 dpONT, $P = 0.3415$; and at 18 dpONT, $P = 0.9416$. ns, $P > 0.1234$; and **** $P \leq 0.0001$.

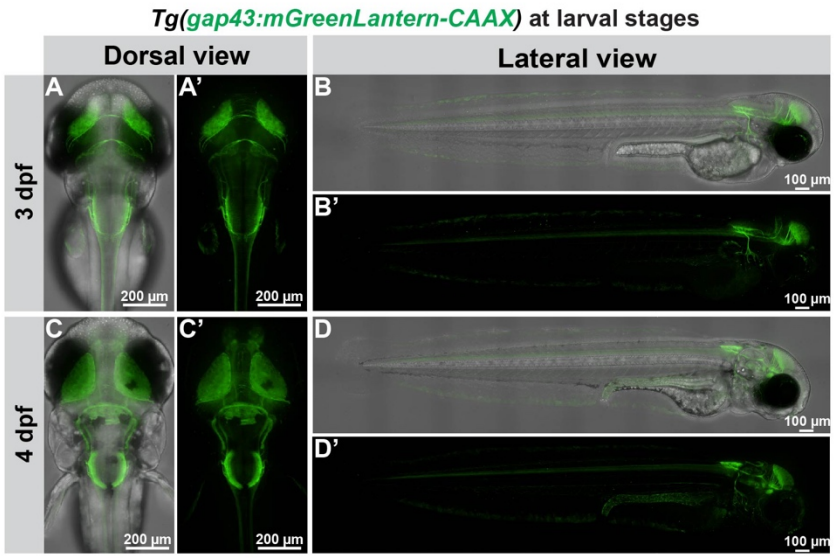

Extended Data 3. *gap43* reporter expression in *Tg(gap43:mGreenLantern-CAAX)* larvae. (A-D) *gap43* reporter expression (green channel) merged with the corresponding bright field image at the time-point indicated. dpf = days post fertilization **(A'-D')** *gap43* reporter expression only (green channel) at the time-point indicated. (A-A') (C-C') Maximum intensity projection (MIP) images of the dorsal view. The total z-stack was 168.30 µm in (A-A') and 226.80 µm in (C-C'). (B-B') (D-D') MIP images of the lateral view. The total z-stack was 199.80 µm. All confocal images were acquired using a 20X objective (N.A. = 0.75, 0.9 µm/step).

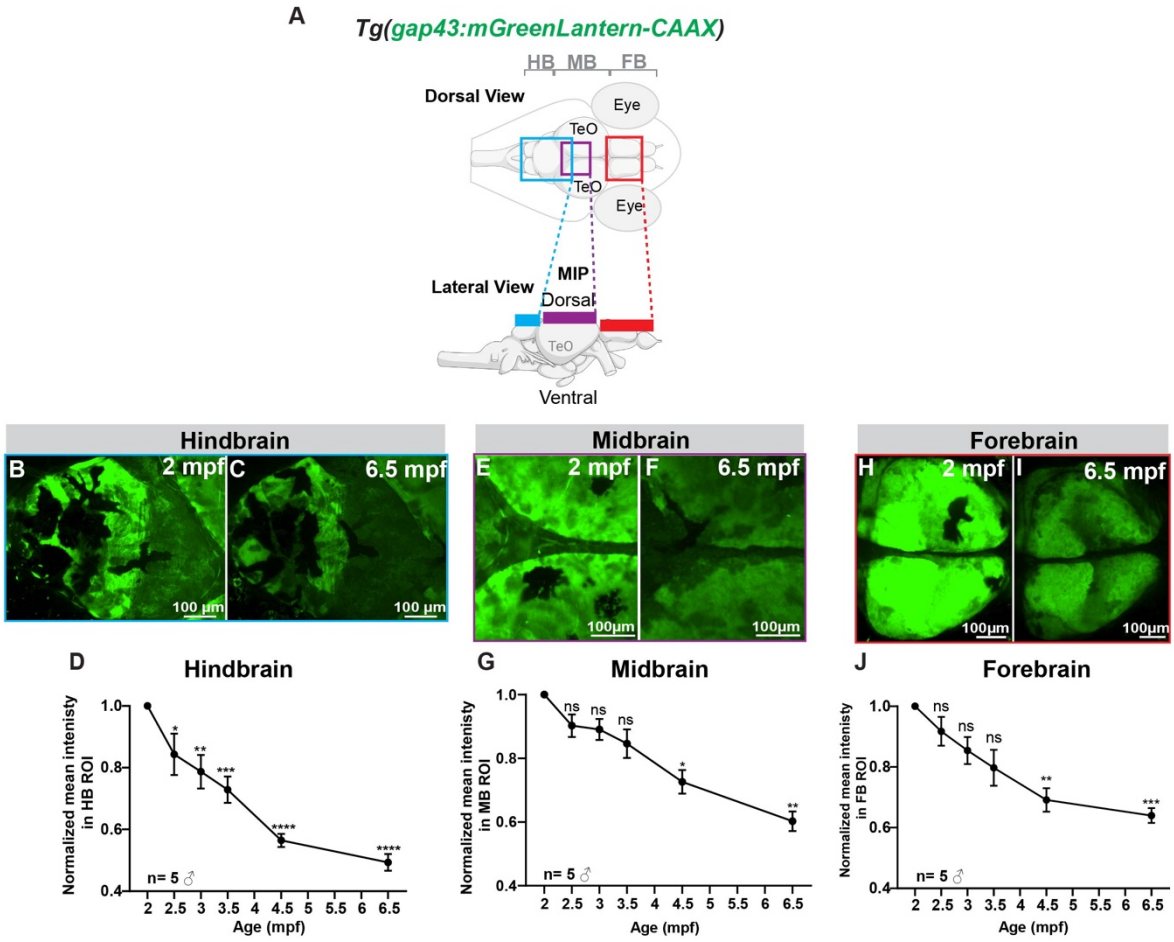

Extended Data 4. Quantifying levels of *gap43* reporter expression in adult *D. cerebrum*. **(A)** Illustration showing the regions imaged in the hindbrain (HB; B-C), midbrain (MB; E-F), and forebrain (FB; H-I). The colored boxes indicated the approximate areas covered in each region. All confocal images were acquired with a 20X objective (N.A. = 0.75, 1.8 µm/z-step) and presented as maximum intensity projections (MIPs). TeO= optic tectum and ♂ = Male. **(B-C)** Dorsal view MIPs of the HB at 2- and 6.5-months post fertilization (mpf). The total z-stack was 110 µm thick. **(D)** Quantification of mean signal intensity from gap43-driven expression (normalized to levels at 2 mpf) in adult transgenic animals. All data represented as mean ±SEM (n = 5). *P* values of each time-point were calculated against the 2 mpf time-point using Repeated Measures 1-way ANOVA (*P* values from left to right: $P = 0.0357$, $P = 0.0055$, $P = 0.0008$, $P = <0.0001$, and $P = <0.0001$. ns, $P > 0.1234$; * $P \leq 0.0332$; ** $P \leq 0.0021$; *** $P \leq 0.0002$; and **** $P \leq 0.0001$. **(E-F)** Dorsal view MIPs of the MB at 2 and 6.5 mpf. The total z-stack was 95.4 µm thick. **(G)** Quantification of mean signal intensity from gap43-driven expression (normalized to levels at 2 mpf) in adult transgenic animals. All data represented as mean ±SEM (n = 5). *P* values of each time-point were calculated against the 2 mpf time-point using Repeated Measures 1-way ANOVA (*P* values from left to right: $P = 0.5718$, $P = 0.1548$, $P = 0.1351$, $P = 0.0076$, and $P = 0.0007$. ns, $P > 0.1234$; * $P \leq 0.0332$; and ** $P \leq 0.0021$. **(H-I)** Dorsal view MIPs of the FB at 2 and 6.5 mpf. The total z-stack was 228.6 µm thick. **(J)** Quantification of mean signal intensity from gap43-driven expression (normalized to levels at 2 mpf) in adult transgenic animals. All data represented as mean ±SEM (n=5). *P* values of each time-point was calculated against the 2 mpf time-point using Repeated Measures one-way ANOVA (*P* values from left to right: $P = 0.2412$, $P = 0.1490$, $P = 0.1348$, $P = 0.0104$, and $P = 0.0012$). ns, $P > 0.1234$; ** $P \leq 0.0021$; and *** $P \leq 0.0002$.

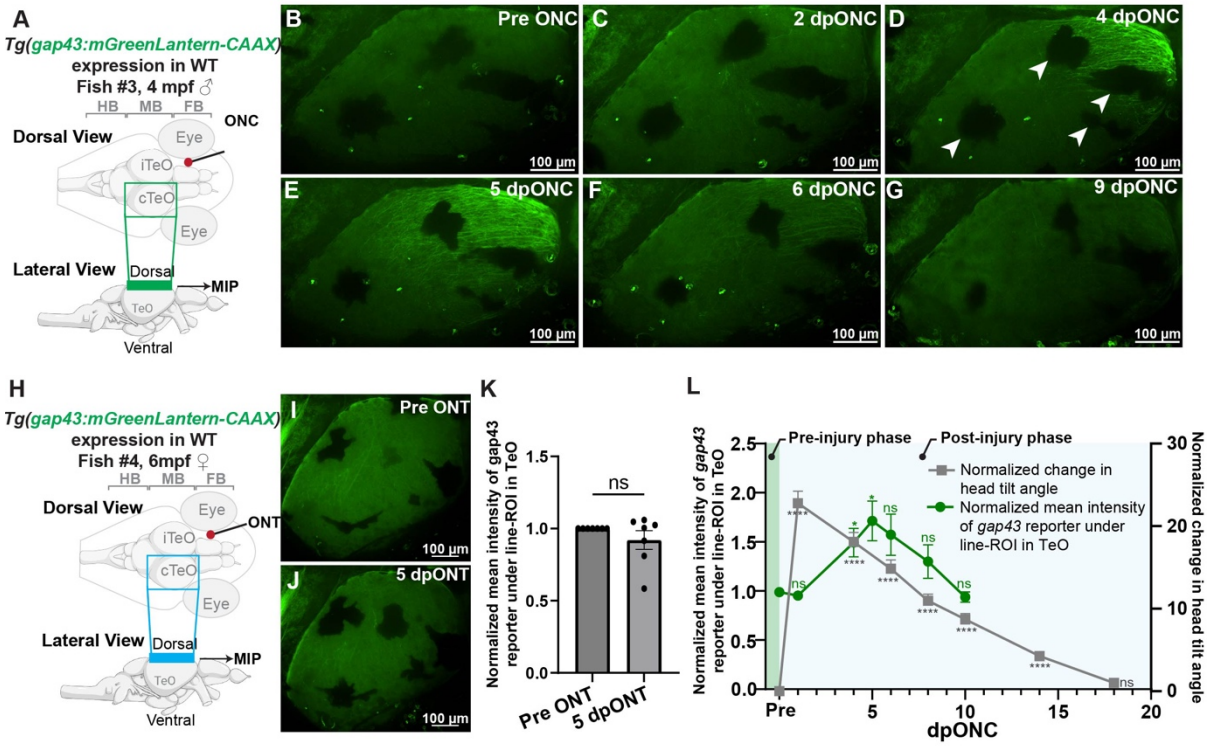

Extended Data 5. Characterizing *gap43* reporter expression after optic nerve injuries. (A) Schematic representation of brain region imaged in B-G before and after an optic nerve crush (ONC) injury. FB = Forebrain, MB = Midbrain, HB = Hindbrain, TeO = optic tectum, cTeO = contralateral TeO, iTeo = ipsilateral TeO and ♂ = Male. **(B-G)** Confocal maximum intensity projection (MIP) images at the time-points indicated were acquired using a 10X objective (N.A. = 0.45, 2.5 µm/z-step) in a *Tg(gap43:mGreenLantern-CAAX)* male at 4-months post fertilization (mpf) and 1.35 cm in length. dpONC = days post ONC. White arrowheads in (D) indicate pigment cells. **(H)** Schematic representation of brain region imaged in J-K before and 5-days post optic nerve transection (dpONT) injury. ♀ = female **(I-J)** MIP images acquired at the time-point indicated using a 10X objective (N.A. = 0.45, 2.5 µm/z-step) in a *Tg(gap43:mGreenLantern-CAAX)* female at 6 mpf and 1.50 cm in length. **(K)** Mean intensity of *gap43* expression in the TeO before and 5 dpONT. Values were normalized to pre ONT readings and expressed as arbitrary units. All data represented as mean ±SEM (n = 6). *P* value was calculated using a 2 Tailed Paired t-test. ns, $P = 0.2689$. **(L)** Correlation between *gap43* expression and head tilt angles measured using the DLR assay before and after an ONC injury. Values were normalized to pre ONC readings and expressed as arbitrary units (gap43 reporter expression) or angle (head tilt). (n = 16, the same group of fish were used for *gap43* and DLR analysis). All data represented as mean ±SEM. *P* values were calculated using Mixed Effects Repeated Measures 2-way ANOVA. *P* values represented as compared to pre ONC. For the gray line: *P* values from left to right: $P = <0.0001$, $P = <0.0001$, $P = <0.0001$, $P = <0.0001$, $P = <0.0001$, $P = <0.0001$, and $P = 0.5676$. For the green line: *P* values from left to right: $P = 0.9728$, $P = 0.0446$, $P = 0.0346$, $P = 0.1417$, $P = 0.5474$, and $P = 0.9576$. ns, $P > 0.1234$; * $P \leq 0.0332$; *** $P \leq 0.0002$; and **** $P \leq 0.0001$.

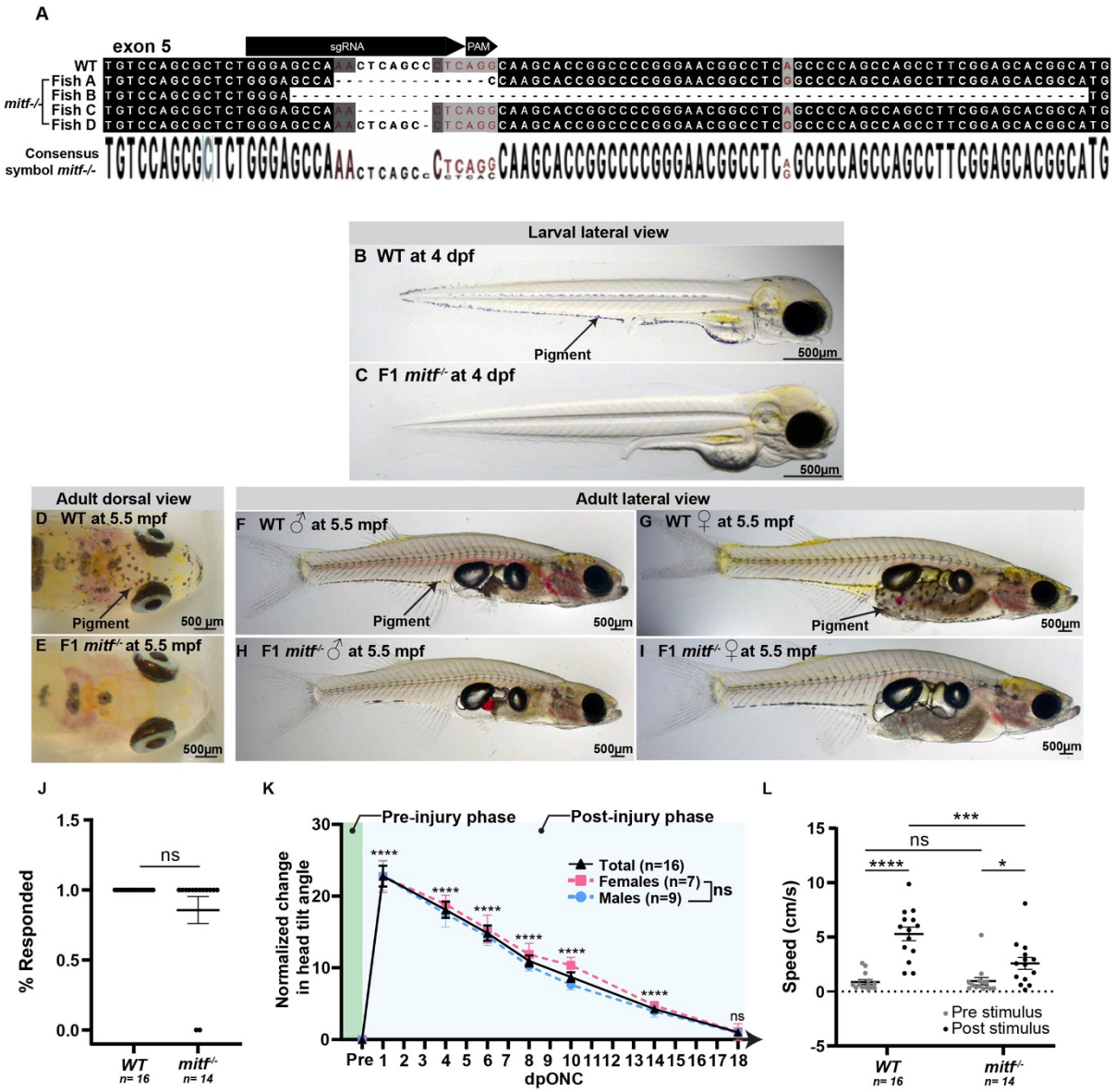

Extended Data 6. Generating a *D. cerebrum mitf* $^{-/-}$ pigment deficient line and evaluating vision in adult mutant fish. (A) Targeted region within exon 5 of the *mitf* gene. Sequence alignment comparing the *wild-type* (*WT) mitf* sequence to indels of isolated (founder) *mitf*$^{-/-}$ fish. The sequence of the targeting gRNA is indicated. **(B)** Lateral view of larval *WT D. cerebrum* at 4-days post fertilization (dpf). Black arrow indicates the pigment spots on the ventral side of the larva. **(C)** Lateral view of larval *mitf*$^{-/-}$ *D. cerebrum* at 4 dpf. **(D)** Dorsal view of an adult *WT D. cerebrum* at 5.5-months post fertilization (mpf). Black arrow indicates a pigment spot. **(E)** Dorsal view of an adult *mitf*$^{-/-}$*D. cerebrum* at 5.5 mpf. (**F-G)** Lateral view of an adult *WT D. cerebrum* male (F) and female (G) at 5.5 mpf. Black arrow indicates pigment. **(H-I)** Lateral view of an adult *mitf*$^{-/-}$ *D. cerebrum* male (H) and female (I) at 5.5 mpf. ♀ = female and ♂ = Male **(J)** Results of the LR assay comparing WT to *mitf*$^{-/-}$ fish. All data represented in mean ±SEM (n = 16 *WT* and n = 14 *mitf*$^{-/-}$). *P* value was calculated using 2 Tailed Unpaired t-test. ns, *P* = 0.1259. **(K)** DLR assay performed on adult *mitf*$^{-/-}$ fish. Head tilt angle was measured before injury and over 18 dpONC. Post injury values were normalized to Pre ONC levels. All data represented in mean ±SEM. Black dotted line represents all animals (n = 16), pink dotted line represents the females (n=7), blue dotted line represents the males (n = 9). *P* values of all animals (total) at each time-points compared to pre ONC from left to right: *P* = <0.0001, *P* = <0.0001, *P* = <0.0001, *P* = <0.0001, *P* = <0.0001, *P* = <0.0001, and *P* = 0.5676. For females vs males, at 1 dpONC, *P* = 0.9997; at 4 dpONC, *P* = 0.8123; at 6 dpONC, *P* =

0.9025; at 8 dpONC, P = 0.6330; at 10 dpONC P = 0.1571; at 14 dpONC P = 0.6844; and 18 dpONC P = 0.9912. ns, P > 0.1234; and **** $P \leq 0.0001$. **(L)** Swim speed (cm/s) was averaged over 1s after the LR stimulus in *WT* and *mitf*$^{-/-}$ fish. All data represented in mean ±SEM (n=16 *WT* and n=14 *mitf*$^{-/-}$). P value was calculated using Repeated Measures 2-Way ANOVA. *WT* pre vs post stimulus, P = <0.0001; *mitf*$^{-/-}$ pre vs post stimulus, P = 0.0153; Pre stimulus *WT* vs *mitf*$^{-/-}$, P= 0.9050; and Pre stimulus *WT* vs *mitf*$^{-/-}$, P= 0.0001. ns, P > 0.1234; * $P \leq 0.0332$; *** $P \leq 0.0002$; and **** $P \leq 0.0001$.

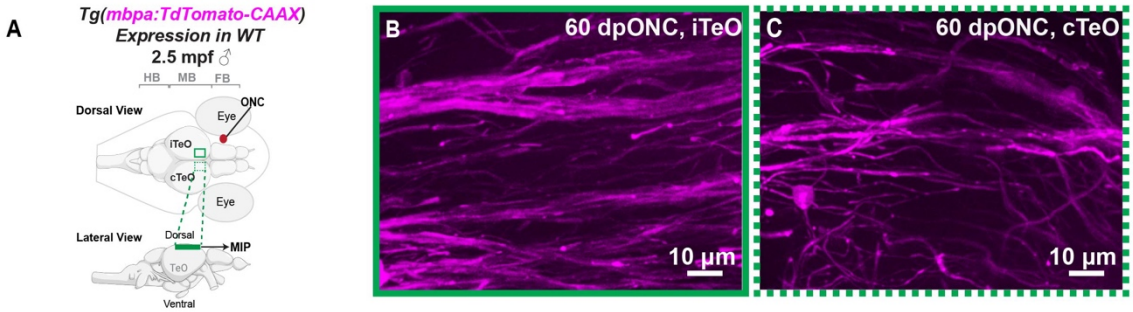

Extended Data 7. Myelination in the optic Tectum (TeO) 60 days after an ONC injury. (A) Schematic illustration of the brain regions imaged and shown in B and C. Green boxes indicate the approximate areas imaged. Images presented as maximum intensity projections (MIPs). FB = Forebrain, MB = Midbrain, HB = Hindbrain, cTeO = contralateral TeO and iTeo = ipsilateral TeO and ♂ = male. **(B-C)** Images were acquired at 60 dpONC with a 40X objective (N.A. = 1.15, 0.4 µm/z-step) in a male *Tg(mbpa:TdTomato-CAAX)* at 4.5-months post fertilization (mpf) 1.37 cm in length. The total z-stack used for MIP was 56.8 µm.

References

1. Park, K.K. *et al.* Promoting axon regeneration in the adult CNS by modulation of the PTEN/mTOR pathway. *Science* 322, 963-966 (2008).
2. Belin, S. *et al.* Injury-induced decline of intrinsic regenerative ability revealed by quantitative proteomics. *Neuron* 86, 1000-1014 (2015).
3. Schaeffer, J., Vilallongue, N., Belin, S. & Nawabi, H. Axon guidance in regeneration of the mature central nervous system: step by step. *Neural Regeneration Research* 18, 2665-2666 (2023).
4. Lim, J.H. *et al.* Neural activity promotes long-distance, target-specific regeneration of adult retinal axons. *Nat Neurosci* 19, 1073-1084 (2016).
5. Daeschler, S.C., Zhang, J., Gordon, T. & Borschel, G.H. Optical tissue clearing enables rapid, precise and comprehensive assessment of three-dimensional morphology in experimental nerve regeneration research. *Neural Regen Res* 17, 1348-1356 (2022).
6. Chato-Astrain, J., García-García, Ó.D., Campos, F., Sánchez-Porras, D. & Carriel, V. Basic Nerve Histology and Histological Analyses Following Peripheral Nerve Repair and Regeneration, in *Peripheral Nerve Tissue Engineering and Regeneration*. (eds. J.B. Phillips, D. Hercher & T. Hausner) 151-187 (Springer International Publishing, Cham; 2022).
7. Suthya, A.R., Wong, C.H.Y. & Bourne, J.H. Diving head-first into brain intravital microscopy. *Front Immunol* 15, 1372996 (2024).
8. Murashova, L. & Dyachuk, V. Modeling traumatic brain and neural injuries: insights from zebrafish. *Front Mol Neurosci* 18, 1552885 (2025).
9. Britz, R., Conway, K.W. & Rüber, L. The emerging vertebrate model species for neurophysiological studies is Danionella cerebrum, new species (Teleostei: Cyprinidae). *Sci Rep-Uk* 11, 18942-18942 (2021).
10. Lam, P.Y. Longitudinal in vivo imaging of adult Danionella cerebrum using standard confocal microscopy. *Dis Model Mech* 15 (2022).
11. Penalva, A. *et al.* Establishment of the miniature fish species Danionella translucida as a genetically and optically tractable neuroscience model. *bioRxiv* (2018).
12. Schulze, L. *et al.* Transparent Danionella translucida as a genetically tractable vertebrate brain model. *Nat Methods* 15, 977-983 (2018).
13. Lindemann, N. *et al.* A comparative analysis of Danionella cerebrum and zebrafish (Danio rerio) larval locomotor activity in a light-dark test. *Front Behav Neurosci* 16, 885775 (2022).
14. Lee, T.J. & Briggman, K.L. Visually guided and context-dependent spatial navigation in the translucent fish Danionella cerebrum. *Curr Biol* 33, 5467-5477 e5464 (2023).
15. Vasconcelos, R.O. *et al.* Characterization of the vocal behavior of the miniature and transparent fish model, Danionella cerebruma). *J Acoust Soc Am* 155, 781-789 (2024).
16. Zada, D. *et al.* Development of neural circuits for social motion perception in schooling fish. *Curr Biol* 34, 3380-3391 e3385 (2024).
17. Cook, V. *et al.* Ultrafast sound production mechanism in one of the smallest vertebrates. *Proc Natl Acad Sci U S A* 121, e2314017121 (2024).
18. Groneberg, A.H., Dressler, L.E., Kadobianskyi, M., Muller, J. & Judkewitz, B. Development of sound production in Danionella cerebrum. *J Exp Biol* 227 (2024).
19. Veith, J. *et al.* The mechanism for directional hearing in fish. *Nature* 631, 118-124 (2024).
20. Rajan, G. *et al.* Evolutionary divergence of locomotion in two related vertebrate species. *Cell Rep* 38, 110585 (2022).
21. Penalva-Tena, A. *et al.* Oxytocin-mediated social preference and socially reinforced reward learning in the miniature fish Danionella cerebrum. *Current Biology*.
22. Williams, P.R., Benowitz, L.I., Goldberg, J.L. & He, Z. Axon Regeneration in the Mammalian Optic Nerve. *Annu Rev Vis Sci* 6, 195-213 (2020).

23. Bormann, P., Zumsteg, V.M., Roth, L.W. & Reinhard, E. Target contact regulates GAP-43 and alpha-tubulin mRNA levels in regenerating retinal ganglion cells. *J Neurosci Res* 52, 405-419 (1998).
24. Zou, S., Tian, C., Ge, S. & Hu, B. Neurogenesis of retinal ganglion cells is not essential to visual functional recovery after optic nerve injury in adult zebrafish. *PLoS One* 8, e57280 (2013).
25. Diekmann, H., Kalbhen, P. & Fischer, D. Characterization of optic nerve regeneration using transgenic zebrafish. *Front Cell Neurosci* 9, 118 (2015).
26. Udvadia, A.J. 3.6 kb genomic sequence from Takifugu capable of promoting axon growth-associated gene expression in developing and regenerating zebrafish neurons. *Gene Expr Patterns* 8, 382-388 (2008).
27. Beckers, A., Bergmans, S., Van Dyck, A. & Moons, L. Analysis of Visual Recovery After Optic Nerve Crush in Adult Zebrafish. *Methods Mol Biol* 2636, 437-447 (2023).
28. Mensinger, A.F. & Powers, M.K. Visual function in regenerating teleost retina following surgical lesioning. *Vis Neurosci* 24, 299-307 (2007).
29. Hu, M. & Veldman, M.B. Srebf2 mediates successful optic nerve axon regeneration via the mevalonate synthesis pathway. *Molecular Neurodegeneration* 20, 28 (2025).
30. Watanabe, S., Takabayashi, A., Takagi, S., von Baumgarten, R. & Wetzig, J. Dorsal light response and changes of its responses under varying acceleration conditions. *Adv Space Res* 9, 231-240 (1989).
31. Lindsey, A.E. & Powers, M.K. Visual behavior of adult goldfish with regenerating retina. *Vis Neurosci* 24, 247-255 (2007).
32. Temizer, I., Donovan, J.C., Baier, H. & Semmelhack, J.L. A Visual Pathway for Looming-Evoked Escape in Larval Zebrafish. *Curr Biol* 25, 1823-1834 (2015).
33. Dunn, T.W. *et al.* Neural Circuits Underlying Visually Evoked Escapes in Larval Zebrafish. *Neuron* 89, 613-628 (2016).
34. Nevin, L.M., Robles, E., Baier, H. & Scott, E.K. Focusing on optic tectum circuitry through the lens of genetics. *BMC Biol* 8, 126 (2010).
35. Karimi-Abdolrezaee, S., Verge, V.M. & Schreyer, D.J. Developmental down-regulation of GAP-43 expression and timing of target contact in rat corticospinal neurons. *Exp Neurol* 176, 390-401 (2002).
36. Reinhard, E., Nedivi, E., Wegner, J., Skene, J.H. & Westerfield, M. Neural selective activation and temporal regulation of a mammalian GAP-43 promoter in zebrafish. *Development* 120, 1767-1775 (1994).
37. Lister, J.A., Robertson, C.P., Lepage, T., Johnson, S.L. & Raible, D.W. nacre encodes a zebrafish microphthalmia-related protein that regulates neural-crest-derived pigment cell fate. *Development* 126, 3757-3767 (1999).
38. Dow, K.E., Levine, R.L., Solc, M.A., DaSilva, O. & Riopelle, R.J. Axonal transport of proteoglycans in regenerating goldfish optic nerve. *Exp Neurol* 126, 129-137 (1994).
39. Ben Fredj, N. *et al.* Synaptic activity and activity-dependent competition regulates axon arbor maturation, growth arrest, and territory in the retinotectal projection. *J Neurosci* 30, 10939-10951 (2010).
40. Li, J., Miramontes, T.G., Czopka, T. & Monk, K.R. Synaptic input and Ca2+ activity in zebrafish oligodendrocyte precursor cells contribute to myelin sheath formation. *Nature Neuroscience* 27, 219-231 (2024).
41. Karttunen, M.J., Czopka, T., Goedhart, M., Early, J.J. & Lyons, D.A. Regeneration of myelin sheaths of normal length and thickness in the zebrafish CNS correlates with growth of axons in caliber. *PLoS One* 12, e0178058 (2017).
42. Hughes, A.N. & Appel, B. Microglia phagocytose myelin sheaths to modify developmental myelination. *Nat Neurosci* 23, 1055-1066 (2020).
43. Zou, S.-q. *et al.* Chapter 2 - Functional Regeneration and Remyelination in the Zebrafish Optic Nerve, in *Neural Regeneration*. (eds. K.-F. So & X.-M. Xu) 21-41 (Academic Press, Oxford; 2015).

44. Münzel, E.J., Becker, C.G., Becker, T. & Williams, A. Zebrafish regenerate full thickness optic nerve myelin after demyelination, but this fails with increasing age. *Acta Neuropathol Commun* 2, 77 (2014).
45. Tsata, V. & Wehner, D. Know How to Regrow-Axon Regeneration in the Zebrafish Spinal Cord. *Cells* 10 (2021).
46. Chowdhury, K., Lin, S. & Lai, S.L. Comparative Study in Zebrafish and Medaka Unravels the Mechanisms of Tissue Regeneration. *Frontiers in Ecology and Evolution* 10 (2022).
47. Lai, S.L., Marín-Juez, R. & Stainier, D.Y.R. Immune responses in cardiac repair and regeneration: a comparative point of view. *Cell Mol Life Sci* 76, 1365-1380 (2019).
48. Shimizu, Y. & Kawasaki, T. Differential Regenerative Capacity of the Optic Tectum of Adult Medaka and Zebrafish. *Front Cell Dev Biol* 9, 686755 (2021).
49. Lai, S.L. *et al.* Reciprocal analyses in zebrafish and medaka reveal that harnessing the immune response promotes cardiac regeneration. *Elife* 6 (2017).
50. Varadarajan, S.G. *et al.* Postsynaptic neuronal activity promotes regeneration of retinal axons. *Cell Rep* 42, 112476 (2023).
51. Delpech, C. *et al.* Axon guidance during mouse central nervous system regeneration is required for specific brain innervation. *Developmental Cell* 59, 3213-3228.e3218 (2024).
52. Rodger, J. *et al.* EphA/ephrin-A interactions during optic nerve regeneration: restoration of topography and regulation of ephrin-A2 expression. *Molecular and Cellular Neuroscience* 25, 56-68 (2004).
53. Rodger, J. *et al.* Changing Pax6 expression correlates with axon outgrowth and restoration of topography during optic nerve regeneration. *Neuroscience* 142, 1043-1054 (2006).
54. Filbin, M.T. Axon regeneration: Vaccinating against spinal cord injury. *Current Biology* 10, R100-R103 (2000).
55. Hall, T.E. *et al.* In vivo cell biological screening identifies an endocytic capture mechanism for T-tubule formation. *Nat Commun* 11, 3711 (2020).
56. Kwan, K.M. *et al.* The Tol2kit: a multisite gateway-based construction kit for Tol2 transposon transgenesis constructs. *Dev Dyn* 236, 3088-3099 (2007).
57. Campbell, B.C. *et al.* mGreenLantern: a bright monomeric fluorescent protein with rapid expression and cell filling properties for neuronal imaging. *Proc Natl Acad Sci U S A* 117, 30710-30721 (2020).
58. Oehlers, S.H. *et al.* Interception of host angiogenic signalling limits mycobacterial growth. *Nature* 517, 612-615 (2015).
59. Jung, S.H. *et al.* Visualization of myelination in GFP-transgenic zebrafish. *Dev Dyn* 239, 592-597 (2010).
60. Pinzon-Olejua, A. *et al.* Cre-inducible site-specific recombination in zebrafish oligodendrocytes. *Dev Dyn* 246, 41-49 (2017).
61. Labun, K. *et al.* CHOPCHOP v3: expanding the CRISPR web toolbox beyond genome editing. *Nucleic Acids Res* 47, W171-W174 (2019).
62. Labun, K., Montague, T.G., Gagnon, J.A., Thyme, S.B. & Valen, E. CHOPCHOP v2: a web tool for the next generation of CRISPR genome engineering. *Nucleic Acids Res* 44, W272-276 (2016).
63. Montague, T.G., Cruz, J.M., Gagnon, J.A., Church, G.M. & Valen, E. CHOPCHOP: a CRISPR/Cas9 and TALEN web tool for genome editing. *Nucleic Acids Res* 42, W401-407 (2014).
64. Parvez, S. *et al.* MIC-Drop: A platform for large-scale in vivo CRISPR screens. *Science* 373, 1146-1151 (2021).
65. Lambert, C.J. *et al.* An automated system for rapid cellular extraction from live zebrafish embryos and larvae: Development and application to genotyping. *PLoS One* 13, e0193180 (2018).
66. McKee, A. & McHenry, M.J. The Strategy of Predator Evasion in Response to a Visual Looming Stimulus in Zebrafish (Danio rerio). *Integr Org Biol* 2, obaa023 (2020).

67. Schindelin, J. *et al.* Fiji: an open-source platform for biological-image analysis. *Nature methods* 9, 676-682 (2012).
68. Align Image by line ROI. (2024).
69. Thuma, T.B.T. *et al.* The big warp: Registration of disparate retinal imaging modalities and an example overlay of ultrawide-field photos and en-face OCTA images. *PLoS One* 18, e0284905 (2023).
70. Lowe, D.G. Distinctive image features from scale-invariant keypoints. *International journal of computer vision* 60, 91-110 (2004).
71. Kang, H. Sample size determination and power analysis using the G*Power software. *J Educ Eval Health Prof* 18, 17 (2021).